We are IntechOpen, the world's leading publisher of Open Access books Built by scientists, for scientists

4,800
Open access books available

122,000
International authors and editors

135M
Downloads

Our authors are among the

154
Countries delivered to

TOP 1%
most cited scientists

12.2%
Contributors from top 500 universities

CLARIVATE ANALYTICS BOOK CITATION INDEX INDEXED

WEB OF SCIENCE™

Selection of our books indexed in the Book Citation Index in Web of Science™ Core Collection (BKCI)

Interested in publishing with us?
Contact book.department@intechopen.com

Numbers displayed above are based on latest data collected.
For more information visit www.intechopen.com

20

Design and Development of High-Performance Eco-Mg Alloys

Shae K. Kim
Korea Institute of Industrial Technology
Korea

1. Introduction

The importance of Mg alloy can be clearly expressed by the never ending request for weight reduction to decrease fuel consumption and emission in the transportaion industry. The importance of Mg alloy is also acknowledged in terms of designer's choice due to the unique properties not found in other materials. On the contrary, we can expect the gloomy future of Mg alloy because aluminum, steel, and plastic industries take great effort to keep and/or win back their territory, which in turn suggests that cost plays more and more important role on this situation. As far as I am concerned, I believe that Mg and Al alloys do synergetic effect on the transportation industry in the balance of weight, quality, and cost.

We can approach Mg alloy in this way - considering the questions of 'what is the secret of sustainability?' 'what is the best material for that?' and 'what should we do for Mg alloy?' Mg alloy is the lightest metallic structural material in the world. The resource of Mg alloy is not abundant but unlimited. Mg alloy is inherently recyclable. These 3 points of Mg alloy show fundamentally qualification criteria as the best material for sustainability. However, the need for using SF6 gas or other protective gases and adding toxic Beryllium (Be) and the safety issue of machined chips and products have been the obstacles of Mg alloy for the best sustainable material.

The environmental benefits provided by lightweight, unlimited, and recyclable Mg alloy have the potential to grow significantly in the future if the global Mg members are working together to demonstrate its stewardship by eliminating global warming SF6 or other protective gases and Be addition as well as by ensuring safety during manufacturing and application. It should be done without sacrificing process ability and mechanical property and increasing the life-cycle cost of Mg alloy. This is what Eco-Mg (Environment COnscious magnesium) is all about.

The simple and plain approach of Eco-Mg alloy is to introduce CaO particles in the range of 0.3wt% to 0.7wt% as an ingredient into conventional cast and wrought Mg alloys for (1) non-SF6 process, (2) Be elimination, (3) improved melt cleanliness, (4) ensured original process adjustability for casting, forming, joining as well as surface treatment, (5) improved mechanical property by grain refinement and internal soundness, (6) ensured safety during manufacturing and application by raising oxidation and ignition resistances of machined chips and products, and (7) improved recyclability. CaO of over 0.5~0.7wt% can be introduced for special purposes to develop creep-resistant, fire-retardant or fire-proof,

damping, bio-degradable, desulphurizing Mg alloys. The R&BD fields of Eco-Mg alloy are well illustrated in Figure 1.

There are 2 things to be clearly demonstrated. One thing, indicated in Figure 2, is that Eco-Mg alloy is not only related to CaO. The approach of Eco-Mg alloy promotes alkaline metal oxides such as NaO and KO, alkaline earth metal oxides such as CaO and SrO, and calcium compounds such as CaO, Ca(OH)2, CaC2, CaCN2, CaCO3 and CaSO4 according to the purpose. For commercial applications, CaO, Ca(OH)2, SrO and CaCN2 are now mainly considered.

As illustrated in Figure 3, the other thing is that CaO does not exist as CaO itself in the solidified state. By the reactive phase formation, Mg2Ca phase (C14) in pure Mg and Al2Ca (C15) and/or (Mg, Al)2Ca (C36) phases in Al-bearing Mg alloys are formed. The exceptional difference between Ca and CaO addition is Ca content in α-phase (solid solution phase). It is clear in pure Mg. Although Ca has the strong segregation tendency, Ca added pure Mg solidifies first as α-phase with Ca solid solution and then as divorce eutectic phase of Mg and Mg2Ca, according to Ca content and process condition. On the contrary, CaO added pure Mg alloy solidifies together as α-phase with almost no Ca solid solution and as divorce eutectic phase, regardless of CaO content and process condition. The same phenomena can be obtained with SrO, CaC2 additions in pure Mg and Mg alloys. For example, SrO added Mg alloys generate together α-phase with almost no Sr solid solution and Al4Sr.

This paper will not cover all the aspects of Eco-Mg alloy. Focused only on CaO addition, the general issues of non-SF6 process, process adjustabilities, oxidation and ignition behaviors, and recyclability will be addressed.

2. Non-SF6 process

It is needless to say how important it is not to use SF6 gas during Mg process in terms of global warming potential. There have been 2 approaches for non-SF6 process of Mg melting and casting processes – alternative gas development and alloy development that can be processed without SF6 gas.

There are several alternative gases which have been already developed and actually in the stage of application. The development of alternative gas at current situation is more realistic than alloy development. However, the apporach of alternative gas can not answer the safety of melt cleanliness, machined chips and products, and recyclability.

The research to add metallic Ca into Mg alloy has been carried out for non-SF6 process. It has been revealed to be very useful in terms of non-SF6 process. However, non-SF6 process with Ca added Mg alloy causes another problems such as fluidity decrease, die soldering, and Ca subtraction during recycling. The most serious problem is the change of material property and process condition.

By Non-SF6 process with Eco-Mg alloy, we can simultaneously improve melt quality and fluidity, maintain at least process ajdustability and mechanical property, ensure the safety of machined chips and products, and improve recyclability.

Figure 4 clearly demonstrates the effect of small amount of CaO on non-SF6 casting for pure Mg; and AZ31, AM50, AM60, and AZ91 Mg alloys (Kim et al., 2009; Kim, 2009; Lee, et al., 2007; Lee & Kim, 2008). Figure 4(a) shows the surface changes of pure Mg during casting and solidification under ambient atmosphere without any protective gas. Severe oxidation began and tarnished surface appeared in 10 seconds just after being poured. Severe burning started in 10 seconds and continued even with white flame to the point when all the melt

was consumed by burning. The similar phenomena occurred in AZ31 (Figure 4(c)), AM50 (Figure 4(e)), AM60 (Figure 4(h)), and AZ91 (Figure 4(l)) Mg alloys. It is well known that the continuous oxidation and resultant burning of Mg alloy occur, at high temperature over 500 ^{o}C, due to the porous surface nature of MgO films that do not act as protective layer to prevent further oxidation and burning. The effect of alloying elements on the oxidation and burning resistances is not clear. However, based on the results of Figure 4, the oxidation and burning resistances increase with increasing Al content during casting and solidification, although Al addition cause the decrease of the liquidus and solidus temperatures of Mg alloy. It should be pointed out that the results of Figure 4 are totally different from the oxidation and buring resistances of Mg alloy during oxidation and ignition tests of Mg parts, which will be addressed in chapter 3.1.

Figure 4(b) shows the surface changes of 0.3wt% CaO added pure Mg during casting and solidification under ambient atmosphere without any protective gas. No burning appeared and shiny surfaces were maintained after the solidification was completely stopped. The similar phenomena occurred in AZ31-0.27wt%CaO (Figure 4(d)), AM50-0.27wt%CaO (Figure 4(g)), AM60-0.3wt%CaO (Figure 4(j)), and AZ91-0.27wt%CaO (Figure 4(n)) Mg alloys. The experiments with AM50-0.1wt%CaO (Figure 4(f)), AM60-0.1wt%CaO (Figure 4(i)), and AZ91-0.1wt%CaO (Figure 4(m) Mg alloys were carried out to investigate the minimum amount of CaO for non-SF6 process. The results show that 0.1wt% CaO addition into Mg alloy is not enough to be cast in ambient atmosphere without any protective gas. The further research should be taken to verify the minimum amount of CaO about non-SF6 process for the case of melting and long holding in the furnace, with an emphais on the effect of alloying elements and on various protective conditions such as dry air or nitrogen atmosphere.

Figure 5 shows the as-cast microstructures of pure Mg and AZ31, AM50, AM60, and AZ91 Mg alloys without and with CaO. One thing to be obtained with Eco-Mg alloy is not to sacrifice the original mechanical property of Mg alloy without CaO. Therefore, what is expected by CaO addition is no change in the microstructure, except the grain refinement due to grain-boundary pinning and the internal soundness related to melt cleanliness. The typical microstructures of Mg alloy without CaO under non-equilibrium solidification are the coarse primary α-phase dendrites and bulk skeletal β-phase (Mg17Al12) in the divorced eutectics. The microstructures of Mg alloy with CaO are similar to those without CaO, as mentioned before, except the grain refinement. This is because the grain-boundary consists of β-phase and C15 (Al2Ca), which can be confirmed by the results in Figures 6 and 7 (Lee, et al., 2007; Kim, 2009). The mass fraction of CaO was deduced from Ca mass fraction detected by ICP-mass.

3. Process adjustabilities

3.1 Strip casting adjustability

Figure 8 clearly demonstrates the effect of small amount of CaO on non-SF6 strip casting of AZ31 Mg alloy (Jang, et al., 2008; Kim et al., 2009). Figure 8(a) shows the surface condition of AZ31 Mg alloy strip castings without SF6 gas. The surface was blackened because molten AZ31 Mg alloy reacted with oxygen in the air when the strip left the rolls. Figure 8(b) shows the surface condition of AZ31 Mg alloy strip castings with SF6 gas. In the used prototype strip casting machine, SF6 gas protection was not enough to prevent strip castings from being oxidized. Furthermore, cracks were observed on the surface of the strip castings due

to the adulteration of impurities, which were made by oxidation and burring during strip casting even with SF6 protection. Figure 8(c) shows the surface condition of 0.1wt%CaO added AZ31 Mg alloy strip castings without SF6 gas. Compared with the effect of CaO on gravity casting of AZ31 Mg alloy, 0.1wt%CaO addition was enough for non-SF6 process during strip casting due to the faster cooling rate, that is, the shorter solidification time.
Figure 9 shows the hardness values of the strip castings of AZ31 Mg alloy without and with CaO on the surface area and in the middle section. As planned and expected, the Vickers hardness values of CaO added AZ31 Mg strip castings are similar to those of AZ31 Mg alloy strip castings. The Vickers hardness values are uniform in all the sections.
Figure 10 shows the tensile properties of the strip castings of AZ31 Mg alloy without and with CaO in the as-received condition. The yield strength (YS), ultimate tensile strength (UTS), and elongation (EL) of AZ31 Mg alloy strip castings are 52.0MPa, 161.0MPa and 14.5%, respectively. The YS, UTS and EL of AZ31-0.1wt%CaO Mg alloy strip castings are 87.6MPa, 140.7MPa and 11.7%, respectively. The YS, UTS and EL of AZ31-0.2wt%CaO AZ31 Mg alloy strip castings are 74.9MPa, 175.9MPa and 18.0%, respectively. Not only for non-SF6 process but also for strip casting process optimization, the further research is necessary to verify the optimum amount of CaO and the effect of alloying elements.

3.2 Diecasting adjustability

Figure 11 shows the non-SF6 diecasting process of 0.3wt%CaO added AZ91D Mg alloy under nitrogen atmosphere without SF6 gas (Kim, 2009). Figure 11(b) shows the clean surface of 0.3wt%CaO added AZ91D Mg alloy melt in the open condition of the furnace. The result showed that 0.3wt%CaO was enough for melting, holding, and casting AZ91D Mg alloy only under nitrogen atmosphere wihtout SF6 gas. Figure 11(c) and 11(d) show hot chamber diecasting process for the cellular phone case and mechanical specimens, respectively. Diecasting was performed by using Frech 250-ton hot chamber machine. Figure 12(a) shows the mechanical test specimen of AZ91D Mg alloy diecast under SF_6 and CO_2 atmospheres (Kim, 2009). Figure 12(b) shows the mechanical test specimen of 0.3wt%CaO added AZ91D Mg alloy diecast under nitrogen atmospheres without SF6 gas. Figures 12(c) and 12(d) show the resultanct microstructures of Figures 12(a) and 12(b), respctively. The microstructure of AZ91D Mg alloy consists of porosity and coarse grain, while the grain-refined microstructure of 0.3wt%CaO added AZ91D Mg alloy is obtained with little porosity. Figure 13 shows the hardness values of the mechanical property specimens of Figures 12(a) and 12(b), respectively. The Rockwell hardness values of AZ91D and 0.3wt%CaO added AZ91D Mg alloys are 61.2 and 64.5, respectively. The Rockwell hardness value of 0.3wt%CaO added AZ91D Mg alloy is little higher than that of AZ91D Mg alloy, due to the grain refinement and diespersion stregnthening of Al2Ca phase. Figure 14 shows the tensile properties of AZ91D and 0.3wt%CaO added AZ91D Mg alloys prepared by the process indicated in Figure 12. The yield strengths of AZ91D and 0.3wt%CaO added AZ91D Mg alloys are 151 MPa and 162 MPa, respectively. The yield strength of 0.3wt%CaO added AZ91D Mg alloy is little higher than that of AZ91D Mg alloy, due to the grain refinement and dispersion strengthening of Al2Ca phase. The tensile strengths of AZ91D and 0.3wt%CaO added AZ91D Mg alloys are 242 MPa and 257 MPa, respectively. The improvement of the tensile strength of 0.3wt%CaO added AZ91D Mg alloy is due to the increased yield strength plus the work hardening by the increased elongation. The elongation values of AZ91D and 0.3wt%CaO added AZ91D Mg alloys are 2.96 % and 8 %, respectively. The elongation of 0.3wt%CaO added AZ91D Mg alloy is much higher than

that of AZ91D Mg alloy, due to the soundness of specimem by decreased defects such as oxides, inclusion, and porosity and grain refinement as shown in Figure 12.

Figure 15 shows the non-SF6 cold chamber diecasting process for CaO added AM60 under nitrogen atmosphere without SF6 gas. The diecasting was performed for AM60-(0.25~0.65)wt%CaO Mg alloys by using a Buhler 1,450-ton cold chamber machine as shown in Figure 15(a). Figures 15(b) through 15(d) show the billet preheating system, the clean surface of molten 0.65wt%CaO added AM60 Mg alloy, and oil pan diecasting process. 1-ton of molten AM60 Mg alloy was prepared in a steel crucible heated to 720°C in an electric resistance furnace and then 5kg ingot of 1.2wt%CaO added AM60 Mg alloy was added repeatedly into the furnace. Therefore, the oil pan diecastings with varying CaO content up to 0.65wt% could be diecast. The samples for chemical analysis were prepared at 30-minute interval and the chemical composition was detected by ICP-mass spectrometer. It should be noted that the mechanical test specimens were prepared directly by diecasting even at the end of the product as shown at Figure 16(a). The tensile test specimen has a gauge length of 30mm and a diameter of 6 mm as shown in Figure 16(b).

Figure 17 shows the tensile properties of AM60-(0.25~0.65)wt%CaO Mg alloys prepared by the process indicated in Figure 15. The yield strength, as shown in Figure 17(a), increases linearly with increasing CaO content up to 0.5wt%CaO addition. Over 0.5~0.6wt%CaO addition, the yield strength can be said to be maintained. The highest yield strength at 0.4~0.5wt%CaO addition is 160 MPa and much higher compared with that of AM60 Mg alloy without CaO. The ultimate strength, as shown in Figure 17(b), also increases linearly with increasing content up to 0.5 wt%CaO addition. The highest ultimate strength is 260 MPa at 0.4~0.5 wt%CaO addition. Figure 17(c) shows that the elongation also increases in proportion to CaO content up to 0.4~0.6 wt%CaO addition. The highest elongation value is 16 % at 0.4~0.5wt%CaO addition. Over 0.5~0.6wt%CaO addition, the elongtation can be said to decease due to the higher amount of strengthening phase, Al2Ca.

The yield strength, tensile strength, and elongation of 0.65wt%CaO added AM60 Mg alloy at room temperature are 164 MPa, 260 MPa, and 12 %, respectively. The tensile properties of 0.65wt%CaO added AM60 Mg alloy at 150°C by the cross-head speed of 1mm/min. are 152 MPa, 225 MPa, and 13 %, respectively, as shown in Figure 18. The excellent tensile properties of CaO added AM60 Mg alloy even at 150°C should be carefully revieved by tensile test in diffent cross-head velocity and by creep resistance test.

Figure 19 summarizes the proportional relationship between the strength and elongation of CaO added AM60 Mg alloys, unlike those of AM and AE series Mg alloys. It is common that the optimization of one property by alloying comes at the expense of one or more other properties. A typical example is the relationship of yield strength and ductility. In order to increase yield strength significantly, some ductility has to be sacrificed. The tensile properties of CaO added AM60 Mg alloy at room temperature are greatly improved due to the grain refinement, Al2Ca dispersion strengthening, and increased soundness without oxides, inclusion, and porosity. This can lead to a conclusion that, for a given Al content, controlled CaO addition to AM60 Mg alloy improves both the strength and ductility.

Figure 20 shows the typical microstructures of as-diecast AM60 Mg alloys with (0.2~0.6)wt%CaO. The microstructures are continuously refined with increasing CaO content. The fracture surfaces in Figure 21 also demonstrates that the dimples are demarcated by the intensive slips at grain boundaries in as-diecast AM60 Mg alloys with (0.2~0.6)wt%CaO, unlike the cleavage planes prominently observed in the brittle Mg alloys.

3.3 Extrusion and rolling adjustabilities

The goal of extrusion and rolling adjustabilities for Eco-Mg alloy is to find out minimum amount of CaO that can be processed without SF6 gas during continuous casting and subsequent forming and heat treatment, to apply the same forming conditions, and to maintain mechanical properties of Mg alloy. Figure 22(a) shows the extruded bars of AZ31 Mg alloy without and with CaO (Lee, et al., 2006; Kim, 2007; Kim et al., 2009). The extrusion experiments were done at 350 ^{o}C with the extrusion ratio 20:1 without SF6 gas. The surfaces of all extruded bars are clear. Figure 22(b) shows the relationship between surface roughness and CaO content. The values of surface roughness slightly decrease with increasing CaO content. The surface roughness of AZ31-0.45wt%CaO Mg alloy is flatter than those of AZ31 and AZ31-0.07wt%CaO Mg alloys in part due to the temperature response change. As planned and expected, the Rockwell hardness and tensile properties of the extruded bars of CaO added AZ31 Mg alloy are almost uniform and similar with those of AZ31 Mg alloy extruded bar.

Figure 23 shows the mechanical properties of hot-rolled AZ31 and AZ31-0.3wt%CaO Mg alloys sheets in the as-received condition just after 15-pass hot-rolling without any post heat-treatment. The Rockwell hardness (*F*-scale) values are the same in the both cases, as planned and expected. The hot-rolling experiments were carried out by using a prototype rolling machine. The specimen was preheated at 400 ^{o}C for 20 minutes and the temperature of the rolls was 150 ^{o}C. The reduction ratio per pass was 30% and 15 passes were totally performed.

3.4 Joining adjustability

Friction stir welding was carried out for AZ31 Mg alloy without and with CaO. Butt and laser welding experiments will be expected to be carried out (Ha, et al., 2007; Kim, et al., 2009). Generally, the stir zone of friction stir welded metals is characterized by dynamic recrystallization. As shown in Figures 24(a) and 24(b), the stir zone of AZ31-0.25wt%CaO added AZ31 alloy shows the significantly refined grains compared with that of AZ31 alloy, while the other TMAZ, HAZ, and base metal zone show the similar microstructures for the both cases. It seems that the stir zone of AZ31-0.25wt%CaO Mg alloy was refined in part due to heterogeneous nucleation or grain growth pinning by C15 along the grain-boundary during dynamic recrystallization. The hardness profiles of friction stir welded AZ31 and AZ31-0.25wt%CaO Mg alloys sheets are given in Figure 24(c). There is not a visible difference between AZ31 and AZ31-0.25wt%CaO Mg alloys in TMAZ, HAZ and base metal zone, while, in SZ, the hardness values of AZ31-0.25wt%CaO Mg alloy is much higher than those of AZ31 Mg alloy.

4. Oxidation and ignition behaviors

4.1 Oxidation behavior

Figure 25 shows the weight gain of Mg-Al alloys during oxidation test under dry air atmosphere at 500°C for 7 hours, according to Al content. Pure Mg shows the stable oxidation resistance compared with AZ31 and AM60 Mg alloys. AZ91 Mg alloy shows the poor oxidation resistance. The oxidation resistances of Mg-Al alloys decrease with increasing Al content at 500°C. The effect of Al element on the oxidation resistance of Mg

alloys seems to be attributed to the decrease of the solidus temperature of the alloys. As mentioned in chapter 2, the oxidation resistances of Mg-Al alloys during oxidation test are totally different from the oxidation and burrning resistances during casting and solidification.

Figure 26(a) shows the weight gain of pure Mg and CaO added pure Mg as a function of oxidation time at 500°C for 7 hours (Ha, et al., 2008; Kim, et al., 2009). The results indicate that pure Mg show the parabolic law due to the loose and porous structure of MgO. On the contrary, in CaO added pure Mg, the oxidation rate is reduced with respect to CaO content at the same temperature. Figures 24(b) through 24(e) show the weight gain behaviors of AZ31, AM50, AM60 and AZ91 without and with CaO addition, respectively (Kim, et al., 2005; Kim, et al., 2009; Lee, et al., 2009; Lee & Kim, 2009). As seen in the Figures, the poor oxidation resistances of Mg alloys are exhibited in proportion to the reaction time. The results indicate that Mg alloys show the parabolic law due to the loose and porous structure of MgO. On the contrary, 0.3wt%CaO added AZ31, AM50 and AM60 Mg alloys show the stable oxidation resistances at 500°C, except 0.3wt%CaO added AZ91 Mg alloy with high Al content.

Figure 27 shows the AES depth profiles sputtered form the surface of pure Mg, AM60 and AZ91 without and with CaO. In pure Mg as shown in Figure 27(a), there is the thick MgO layer on the surface because the concentration of Mg and O are constant for sputtering time. In CaO added pure Mg, as shown in Figure 27(b), there is the thin oxide layer mixed with MgO and CaO. The oxidation resistance of CaO added Mg is similar to those of Ca added Mg alloys studied by B. S. You et al (You, 2000). As indicated in Figures 27(c), 27(d), 27(e), and 27(f), the AES depth profiles sputtered from the surfaces of AM60, AM60-0.45wt%CaO, AZ91, and AZ91-0.7wt%CaO Mg alloys after oxidation at 500°C for 7 hours show the similar behaviors like the results of pure Mg and CaO added pure Mg. Generally, MgO layer on the surface of Mg alloys exhibits protective behavior below about 450°C, while the weight gain by oxidation is accelerated with respect to temperature above 450°C, because of the porous naute of MgO surface film at high temperature. It can be explained by Pilling-Bedworth ratio, the ratio of oxide volume to metal volume. Because the Pilling-Bedworth ratio for pure Mg is 0.83, MgO film on the surface of pure Mg can not act as a protective barrier to prevent continuous oxidation. Although it can not be explained by Pilling-Bedworth ratio (Pilling & Bedworth, 1923), it has been reported that the oxidations of Ca added Mg alloys are suppressed due to the dense film mixed with MgO and CaO (0.78).

4.2 Ignition behavior

While the oxidation resistance is related to product performance and durability, the ignition resistance is to the safety and the fear to impede practical application. For the ignition resistance of Mg alloy, the quantitative data is prerequisite. For the quantitative data, the definition and standard test method of the ignition resistance of Mg alloy should be decided.

There are 2 goals for ignition experiments of Eco-Mg alloy. One is to increase the ignition resistance as high as possible with CaO addition for the safety of machined chips and products. The result can be understood with that of non-SF6 process and improved oxidation resistance. The other is to investigate the effect of test method, test environment, and specimen shape on the resistance for obtaining quantitative data. In terms of accuracy,

DTA is the best method. The furnace chip test is useful to verify the safety of machined chips while the torch test is for the safety of products. For the furnace chip test, the thickness of chips, that is, the used tool kinds, the amount of chips, and the degree of compaction should be stated for quantification. The heating rate for DTA test, the furnace temperature for the furnace test, and the flame temperature for the torch test should also be stated.

Figure 28 shows the results of DTA ignition tests of Mg-Al alloys under dry air atmosphere. The ignition temperatures of AZ31, AM60, and AZ91 Mg alloys are 590°C, 560°C, and 559°C, respectively. The ignition temperatures decrease with increasing Al content due to the decrease of the liquidus and solidus temperatures. The similar phenomena are obtained in the oxidation results of Mg-Al Mg alloy as shown in Figure 25.

Figure 29 shows the results of DTA for AZ31, AM60, and AZ91 Mg alloys without and with CaO under dry air atmosphere (Lee, et al., 2007; Lee & Kim, 2008; Lee & Kim, 2009). The ignition temperatures of CaO added Mg alloys increase almost linearly with increasing CaO content. The ignition temperatures of AZ31, 0.32wt%CaO added AZ31, 0.82wt%CaO added AZ31 and 1.22wt%CaO added AZ31 Mg alloys are 590°C, 691°C, 806°C, and 1,177°C, respectively. From the results of DTA for 1.22wt%CaO added AZ31 Mg alloy, it should be noted that fire-proof performance can be controlled by CaO addition. Figures 44(b) and 44(c) show the similar behaviors of CaO added AM60 and AZ91 Mg alloys, respectively.

Figure 30 compares the results of DTA for AZ31, AM60, and AZ91 Mg alloys without CaO and with 1wt% CaO as a function of Al content under dry air atmosphere. The ignition temperatures decrease with increasing Al content without and with CaO. The ignition temperatures of 1wt%CaO added Mg-Al Mg alloys increase by about 300°C in all Mg-Al alloys without CaO. As mentioned before, the effect of Al content can be understood by the liquidus and solidus temperature drops regardless of CaO. The fact that the ignition temperatures increase with increasing CaO content can be understood by the combined effect of the increased oxidation resistance and the decreased Al content to Al2Ca formation in CaO added Mg-Al alloys. Figure 36 clearly demonstrates the changes of solidus and liquidus temperatures with respect to Al and CaO contents in Mg-Al alloys.

Figure 31 shows the results of DTA for commercial high temperature Mg alloys and CaO added Mg-Al Mg alloys under dry air atmosphere. The ignition temperatures of AS21, AE44, MRI153, MRI230, 1.22wt%CaO added AZ31, 1.65wt%CaO added AM60, and 1.5wt%CaO added AZ91 Mg alloys are 591°C, 602°C, 1,057°C, 1,165°C, 1,177°C, 1,161°C, and 1,142°C, respectively. The ignition temperatures of CaO added Mg-Al and MRI230 are over 1,100°C. The ignitions of MRI and CaO added Mg-Al Mg alloys occurred over the liquidus temperatures while AS and AE series Mg alloys ignited below the liquidus temperatures.

Figure 32 shows the chip ignition results of Mg-Al Mg alloys under an ambient atmosphere in the furnace at 800°C. The chip ignition temperatures also decrease with increasing Al content. The chip ignition temperatures of pure Mg, AZ31, AM60, and AZ91 Mg alloys are 602°C, 583°C, 583°C, and 567°C, respectively. Figure 33 shows the effect of CaO on the chip ignition temperatures of pure Mg, AZ31, AM60, and AZ91 Mg alloys under an ambient atmosphere in the furnace at 800°C (Lee, et al., 2007; Lee & Kim, 2008; Lee & Kim, 2009). Figure 33(a) shows the effect of CaO on the chip ignition temperatures of pure Mg. With increasing CaO content, the ignition temperatures of pure Mg increase linearly, as planned and expected. The effect of CaO on the ignition temperatures of AZ31, AM60, and AZ91 Mg

alloys are shown in Figures 33(b), 33(c), and 33(d), respectively. The results say 2 things; one is the possibility to control the ignition temperatures of Mg machined chips and the other is the difficulty to improve much higher the ignition temperatures of Mg alloys in the state of machined chips unlike products. The difference of test atmosphere should be also considered: DTA under dry air atmosphere and furnace chip test under an ambient atmosphere.

Figure 34 shows the chip ignition results of commercial high temperature Mg alloys and CaO added Mg-Al Mg alloys under an ambient atmosphere (Lee & Kim, 2010). The ignition temperatures of AS21, AE44, MRI153, MRI230, 1.22wt%CaO added AZ31, 1.65wt%CaO added AM60, and 1.5wt%CaO added AZ91 Mg alloys are 569°C, 568°C, 584°C, 627°C, 653°C, 638°C, and 604°C, respectively. The ignition temperatures of 1.22wt%CaO added AZ31 and 1.65wt%CaO added AM60 Mg alloys are much higher than those of the other high temperature Mg alloys. The ignition temperatures of MRI230 and CaO added AZ31 and AM60 Mg alloys are only over the liquidus temperatures.

Figure 35 shows the results of torch ignition test for AZ91 and 0.3wt%CaO added AZ91 Mg alloys under an ambient atmosphere (Lee & Kim, 2009). The diecast product was continuously heated by the torch until the ignition occurred. The ignition time was defined at the time when the diecast product was ignited. The ignition times of AZ91 and 0.3wt%CaO added AZ91 Mg alloys are 70 seconds and 210 seconds, respectively. This result might indicate that small CaO addition is of interest for fire-retardant Mg products when they are exposed to fire or spark under an ambient atmosphere. The important point is that the fire of 0.3wt%CaO added AZ91 Mg alloy was extinguished when the torch was turned-off even after the ignition. However, the fire of AZ91 Mg alloy continuously propagated by self-heating. The behavior of the torch ignition results can be discussed from the AES depth profile results. Figure 36 shows the AES depth profiles sputtered from the surface of as-received diecastings. In AZ91 Mg alloy diecastings, there is the thick MgO layer on the surface because the concentration of Mg and O were constant for sputtering time. In 0.3wt%CaO added AZ91 Mg alloy diecastings, on the contrary, there is the thin oxide layers mixed with MgO and CaO.

Figure 37 shows the results of torch ignition test for CaO added Mg-Al alloys and high temperature Mg alloys under an ambient atmosphere (Lee & Kim, 2010). The cast product was continuously heated by the torch until the ignition occurred. The ignition times of 1.13wt%CaO added AZ31, 1wt%CaO added AM60, and 1.02wt%CaO added AZ91 Mg alloys are 200 seconds, 120 seconds, and 120 seconds, respectively. The ignition times of AS21, AE44, MRI153, and MRI230 are 100 seconds, 110 seconds, 100 seconds and 110 seconds, respectively. When the torch was turned-off even after the ignition, the fire of 1.13wt%CaO added AZ31, 1wt%CaO added AM60, 1.02wt%CaO added AZ91, MRI 153, and MRI230 Mg alloys were extinguished. However, the fire of AS21 and AE44 Mg alloys continuously propagated by self-heating.

5. Recyclability

It is well known that Ca in Mg alloys disappears during recycling due to the reaction of Ca with the fluxes. The Ca addition to Mg alloys forms α-phase with Ca solid solution and C14 or C15 phase. As mentioned earlier, CaO addition to Mg alloys forms only C14 or C15 phase as far as Ca is concerned. The goal of flux recycling experiments for Eco-Mg alloy is to verify

separately the reaction of α-phase with Ca solid solution and C14 or C15 phase with each flux. It was confirmed that the flux change could minimize the reduction of Ca content during flux recycling even for Ca added Mg alloys. The suitable fluxes for Mg alloys with C14 and C15 phases are KCl and NaCl without Ca loss.

Figure 38 shows the microstructures of as-cast CaO and Ca added AZ31 Mg alloys. The typical microstructure of as-cast AZ31-0.3wt%Ca Mg alloy is obviously α-phase and irregular β-phase along grain boundaries (Lee & Kim, 2009). The microstructure of as-cast AZ31-0.3wt%CaO Mg alloy is α-phase, irregular β-phase and C15 phase along grain boundaries. Figures 38(b), 38(c), 38(d), 38(e), 38(g), 38(h), 38(i), and 38(j) show the as-recycled microstructures of CaO and Ca added AZ31 Mg alloys after flux recycling by MgCl2, KCl, NaCl, and MnCl2. Table 1 gives the ICP results before and after the recycling of each flux.

The reaction between α-phase with Ca solid solution and MgCl2 is described as $MgCl_2(s) + Ca(s) = CaCl_2(s) + Mg(\ell)$, ΔG_f = -159.943 kJ/mol at 700°C, which explains that the solid solution Ca in AZ31-0.3wt%Ca Mg alloy disappears during recycling because ΔG_f of the reaction is -159.943 kJ/mol. The reactions at 700°C between α-phase and KCl, NaCl, and MnCl2 are described as $2KCl(s) + Ca(s) = CaCl_2(s) + 2K(\ell)$, ΔG_f = +41.401 kJ/mol, $2NaCl(s) + Ca(s) = CaCl_2(s) + 2Na(\ell)$, ΔG_f = -3.773 kJ/mol, and $MnCl_2(s) + Ca(s) = CaCl_2(s) + 2Mn(s)$, ΔG_f = -289.719 kJ/mol. The microstructures, the ICP results, and the thermodynamic equations for the reactions of α-phase with the fluxes indicate the well known fact that the solid solution Ca in Mg alloys disappears during flux recycling.

The reaction of C15 phase with MgCl2 at 700°C is described as $MgCl_2(s) + Al_2Ca(s) = CaCl_2(s) + Mg(\ell) + 2Al(\ell)$, ΔG_f = +45.711 kJ/mol, which explains that C15 phase in AZ31-0.3wt%CaO and AZ31-0.3wt%Ca Mg alloys can be maintained during recycling because ΔG_f of the reaction is +45.711 kJ/mol. The reactions at 700°C between C15 phase and KCl, NaCl, and MnCl2 are described as $2KCl(s) + Al_2Ca(s) = CaCl_2(s) + 2K(\ell) + 2Al(\ell)$, ΔG_f = +247.055 kJ/mol, $2NaCl(s) + Al_2Ca(s) = CaCl_2(s) + 2Na(\ell) + 2Al(\ell)$, ΔG_f = +201.881 kJ/mol, and $MnCl_2(s) + Al_2Ca(s) = CaCl_2(s) + 2Al(\ell) + Mn(s)$, ΔG_f = -84.065 kJ/mol. The microstructures, the ICP results, and the thermodynamic equations for the reactions of C15 with the fluxes well indicate that Ca in the form of C15 phase is not consumed all during conventional flux recycling. With high temperature Mg alloys, Ca in the form of solid solution disappears but Ca in the form of C15 phase could be maintained if the fluxes were selected appropriately. The result clearly demonstrates the superiority of CaO over Ca even for recyclability.

6. Conclusion

We believe that the environmental benefits provided by lightweight, unlimited, and recyclable Mg alloy have the potential to grow significantly in the future by Eco-Mg approach. This paper, regarding CaO as ingredient, described non-SF6 process, process adjustabilities of strip casting, diecasting, extrusion, rolling, and joining, oxidation and ignition resistances, and recyclability of Eco-Mg alloy.

Compared with what have been already accomplished, what will be achieved is much bigger and greater for Eco-Mg alloy. For international cooperation not only for R&D and but also for commercial applications should be carried out.

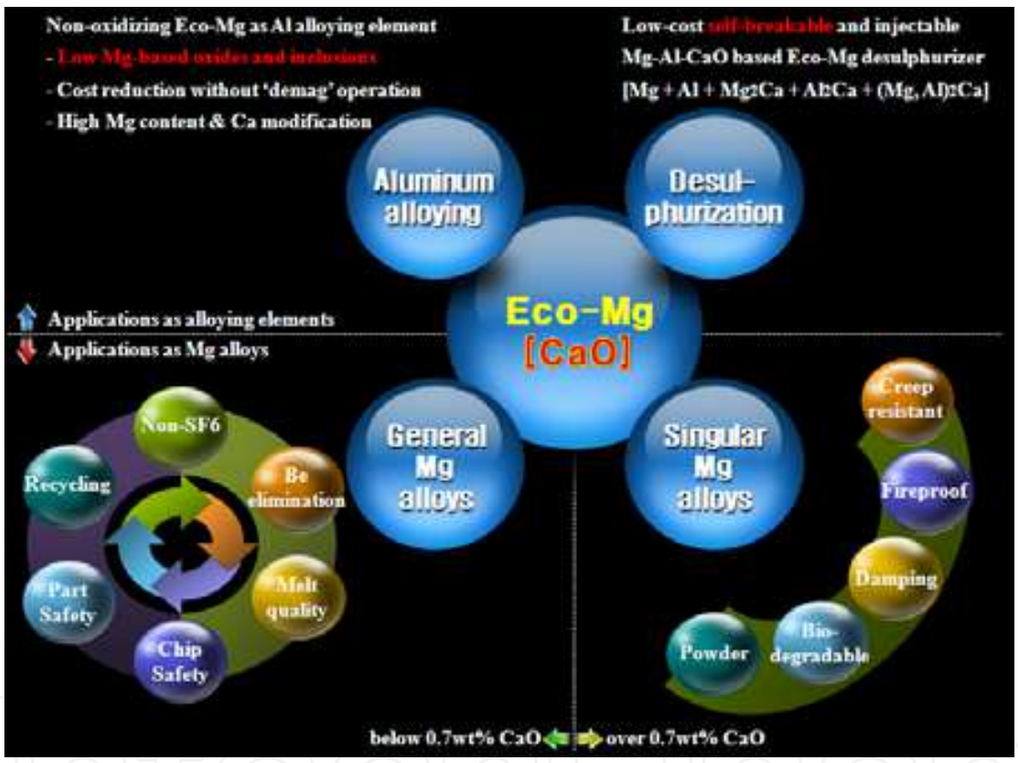

Fig. 1. R&BD fields covered by Eco-Mg utilizing CaO.

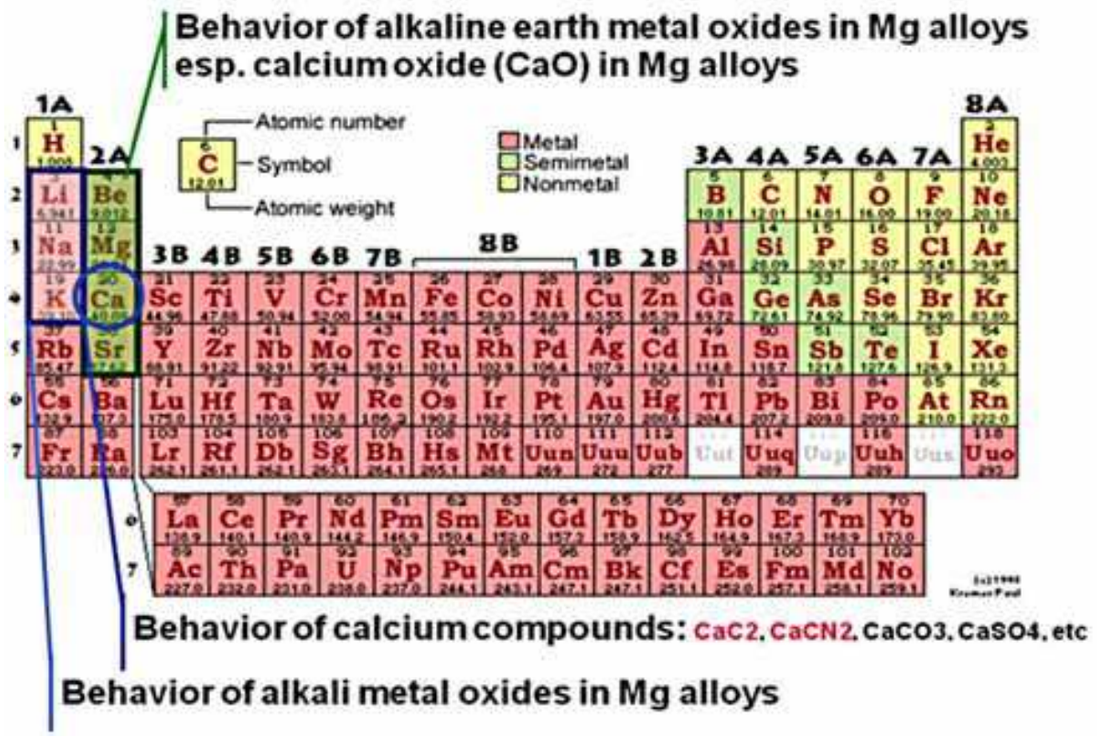

Fig. 2. Research areas covered by Eco-Mg approach.

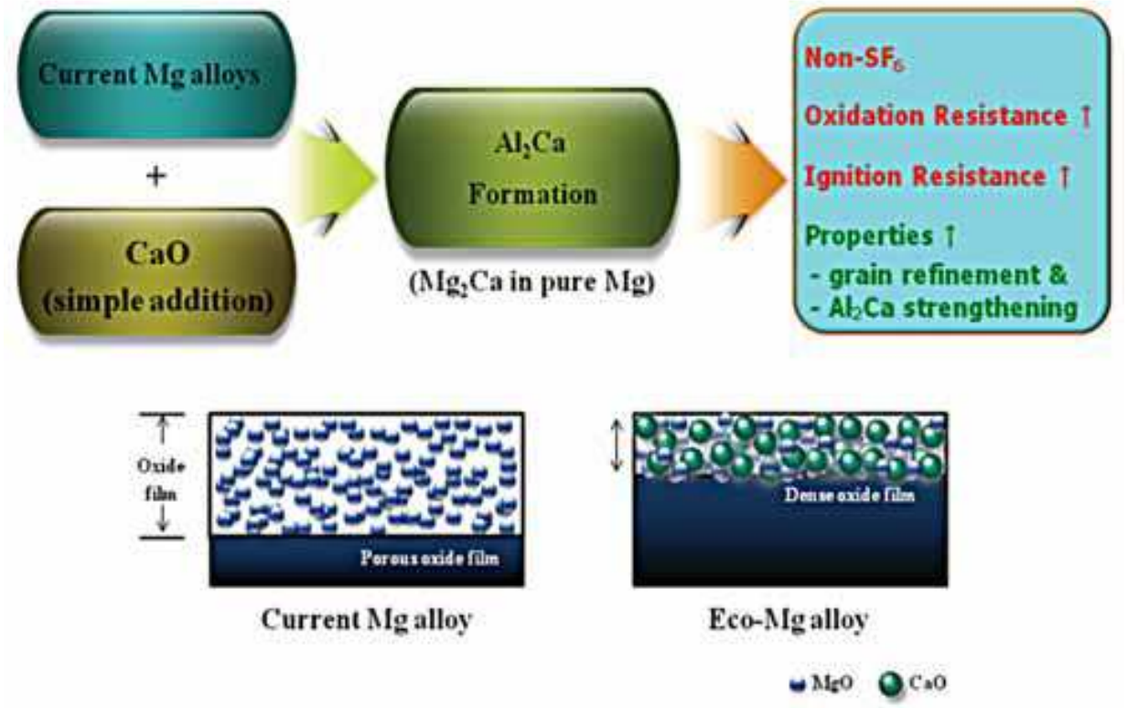

Fig. 3. General introduction, phase formation, surface structure, and resultant effects of CaO added Eco-Mg alloys.

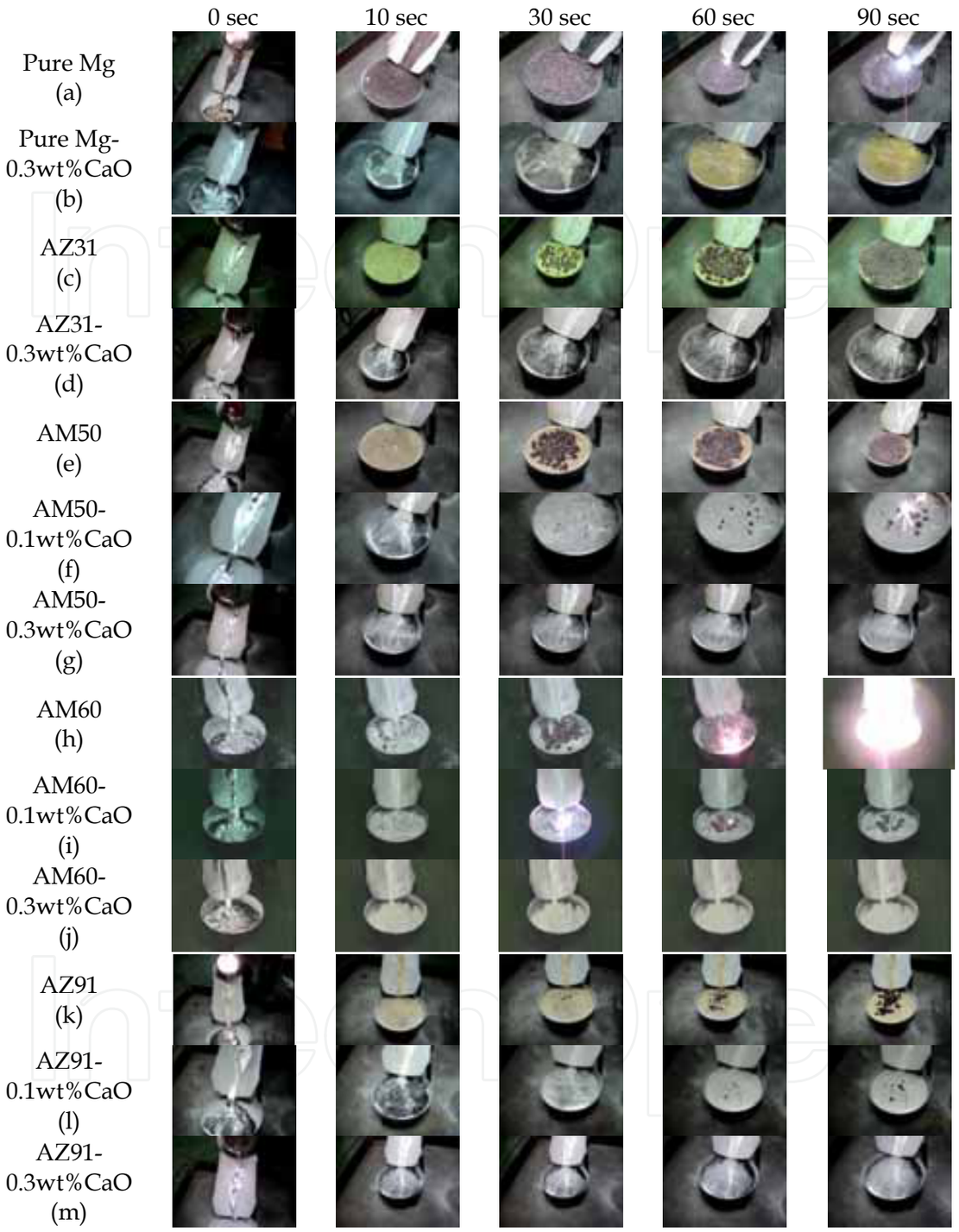

Fig. 4. Surface changes of the (a) pure Mg, (b) pure Mg-0.3wt%CaO, (c) AZ31, (d) AZ31-0.3wt%CaO, (e) AM50, (f) AM50-0.1wt%CaO, (g) AM50-0.3wt%CaO, (h) AM60, (i) AM60-0.1wt%CaO, (j) AM60-0.3wt%CaO, (k) AZ91, (l) AZ91-0.1wt%CaO, and (m) AZ91-0.3wt%CaO during casting and solidification (Kim et al., 2009; Kim, 2009; Lee, et al., 2007; Lee & Kim, 2008).

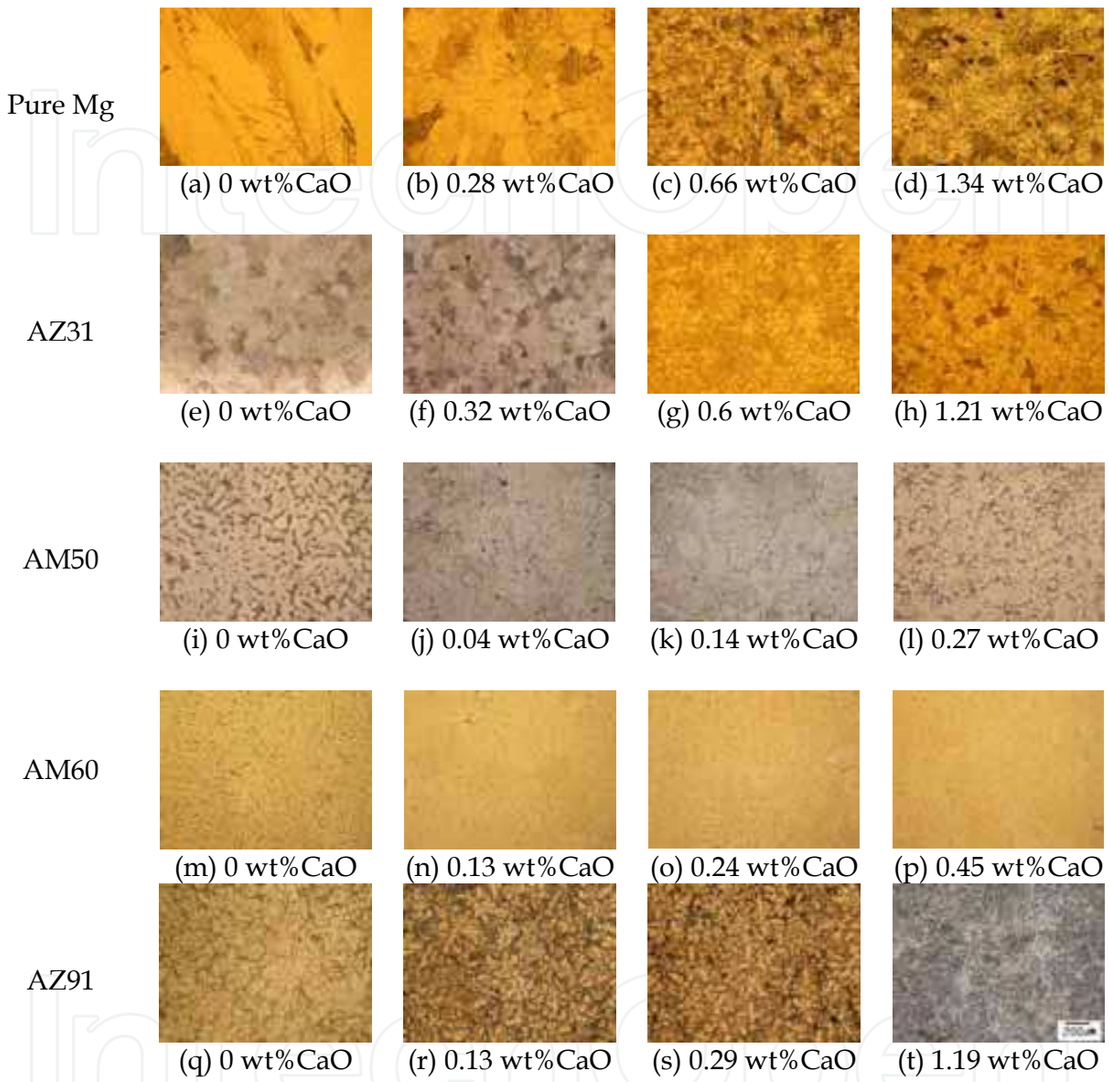

Fig. 5. Microstructures of the (a) pure Mg, (b) pure Mg-0.28wt%CaO, (c) pure Mg-0.66wt%CaO, (d) pure Mg-1.34wt%CaO, (e) AZ31, (f) AZ31-0.32wt%CaO , (g) AZ31-0.6wt%CaO , (h) AZ31-1.21wt%CaO, (i) AM50, (j) AM50-0.04wt%CaO, (k) AM50-0.14wt%CaO, (l) AM50-0.27wt%CaO, (m) AM60, (n) AM60-0.13wt%CaO, (o) AM60-0.24wt%CaO, (p)AM60-0.45wt%CaO, (q) AZ91, (r) AZ91-0.13wt%CaO, (s) AZ91-0.29wt%CaO, and (t) AZ91-1.19wt%CaO (Kim, 2005; Lee, et al., 2007; Ha et al., 2008; Kim et al., 2009).

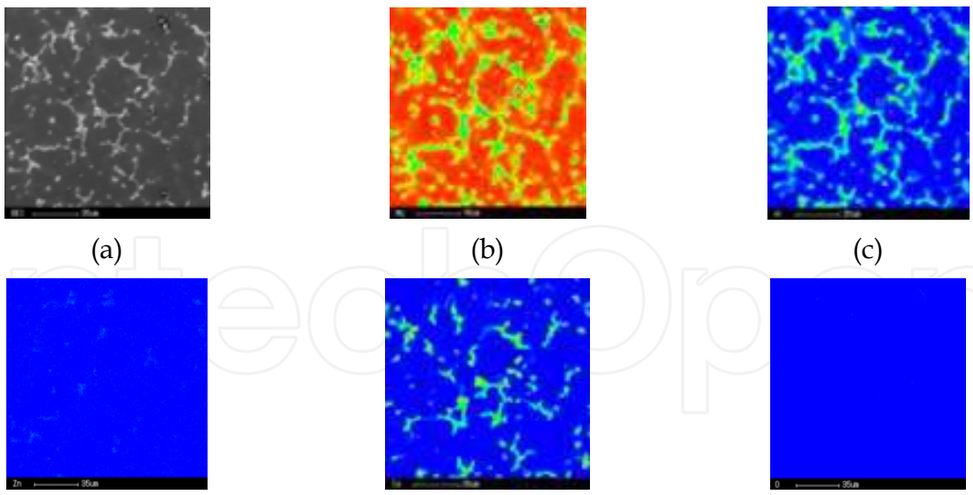

Fig. 6. EPMA mapping results of AZ91-0.29wt%CaO; (a) BE image, (b) Mg, (c) Al, (d) Zn, (e) Ca, and (f) O (Lee, et al., 2007).

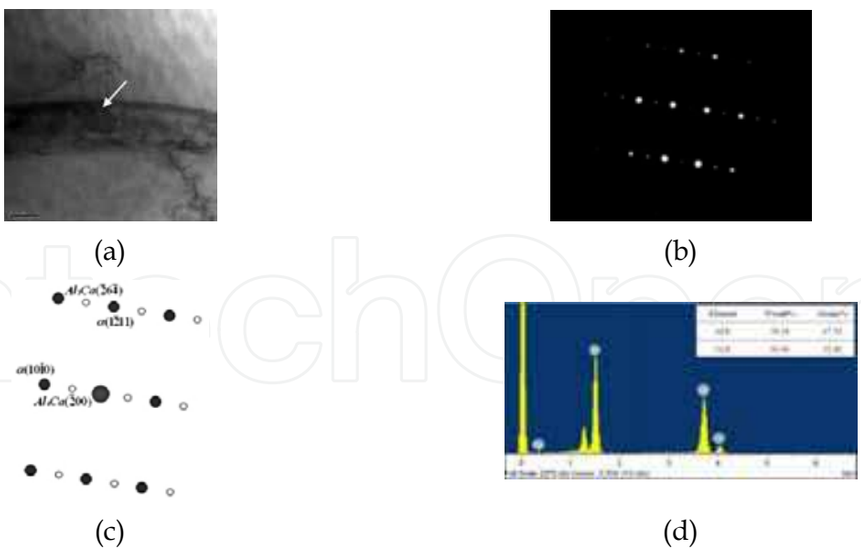

Fig. 7. TEM results of AM50-0.58wt%CaO; (a) BFI, (b) SASD pattern ($Z=[\bar{1}\,2\,\bar{1}\,6]_{\alpha\text{-Mg}}$, $[023]_{Al2Ca}$), (c) the schematic illustration for the SAD pattern, and (d) quantitative elemental analysis (Kim et al., 2009).

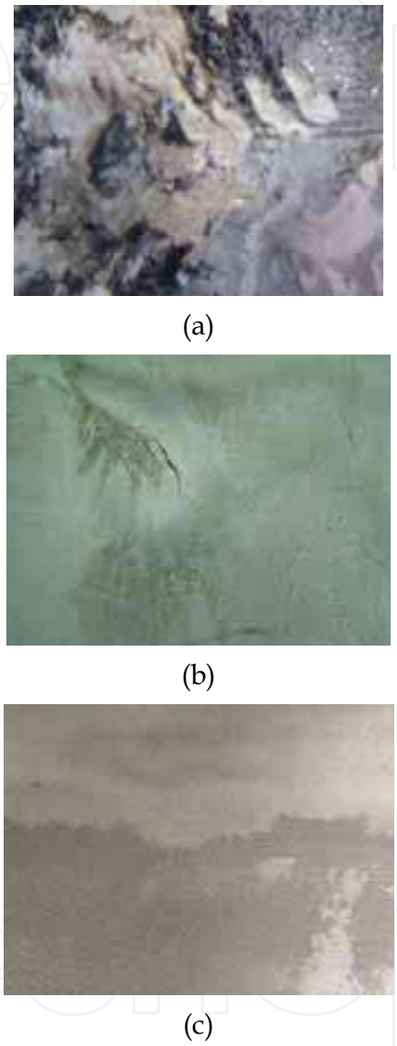

(a)

(b)

(c)

Fig. 8. Surface conditions of as-strip cast (a) AZ31 without SF6 gas, (b) AZ31 with SF6 gas, and (c) AZ31-0.1wt%CaO without SF6 gas (Jang, et al., 2008).

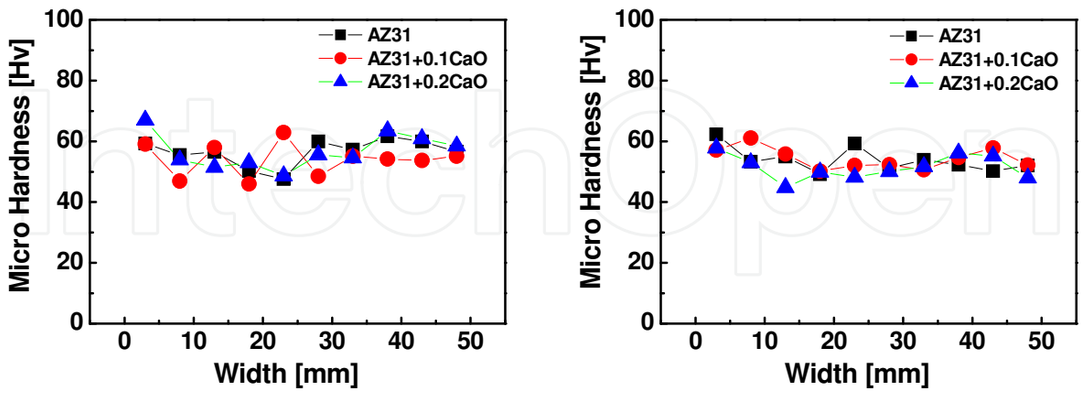

Fig. 9. Hardness values of AZ31, AZ31-0.1wt%CaO and AZ31-0.2wt%CaO strip castings; (a) surface area and (b) middle section of strip castings (Jang, et al., 2008).

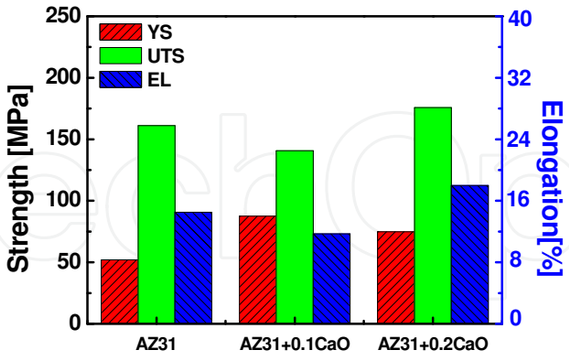

Fig. 10. Mechanical properties of AZ31, AZ31-0.1wt%CaO and AZ31-0.2wt%CaO strip castings (Jang, et al., 2008).

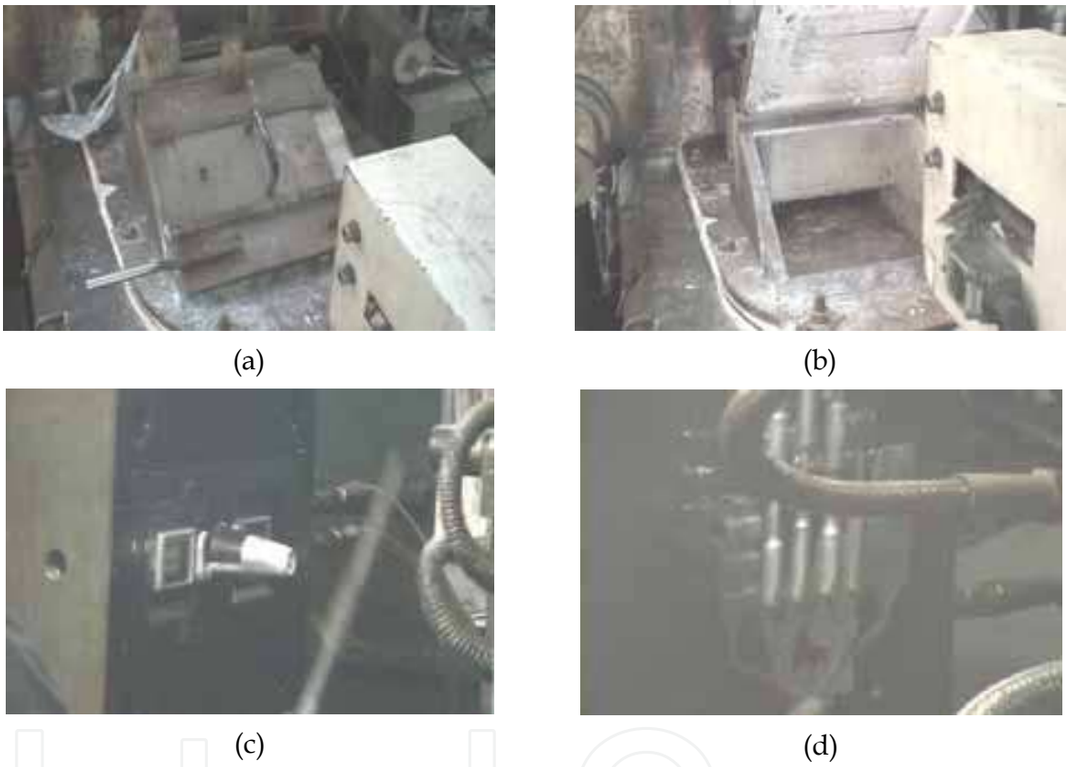

Fig. 11. Non-SF6 diecasting process of AZ91D-0.3wt%CaO under nitrogen atmosphere without any protective gas; (a) close furnace condition, (b) open furnace condition, (c) diecasting of cellular phone case, and (d) diecasting of mechanical test specimen (Kim, 2009).

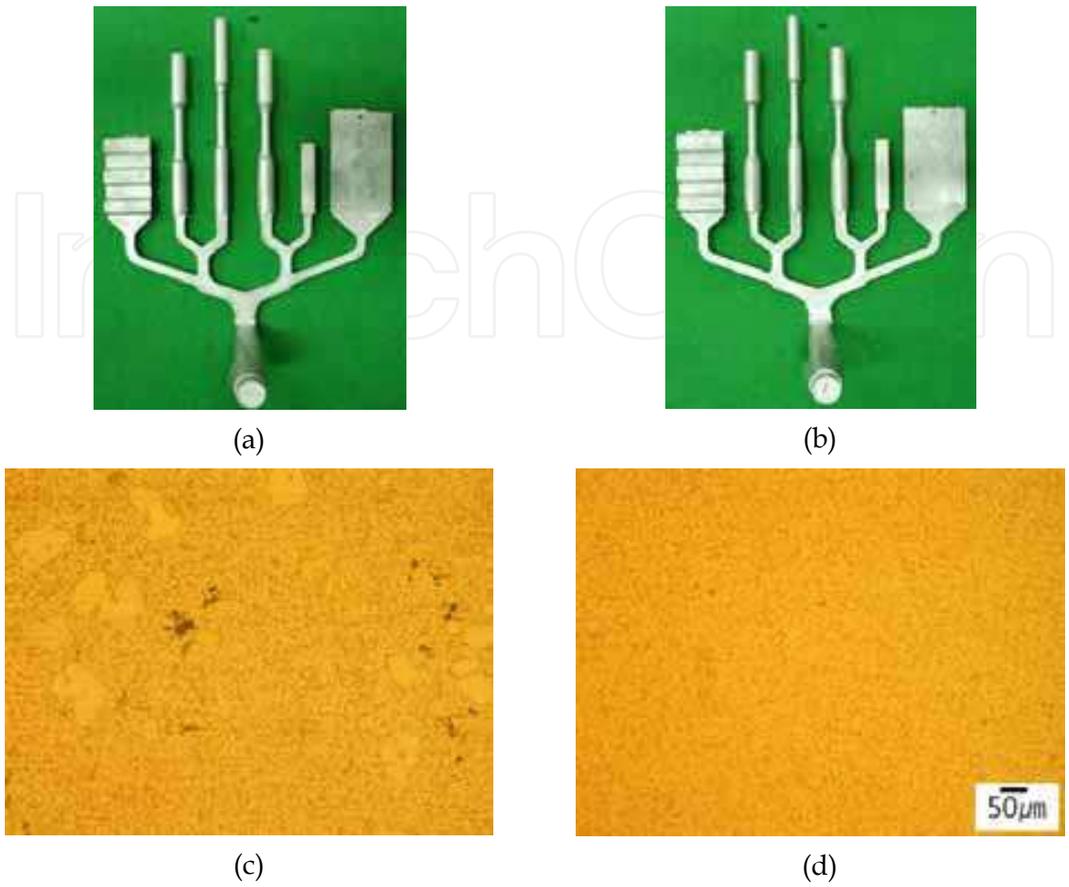

Fig. 12. Photographs of the mechanical test specimens produced by hot chamber diecasting of (a) AZ91D and (b) AZ91D-0.3wt%CaO and the related microstructures of (c) AZ91D and (d) AZ91D-0.3wt%CaO (Kim, 2009).

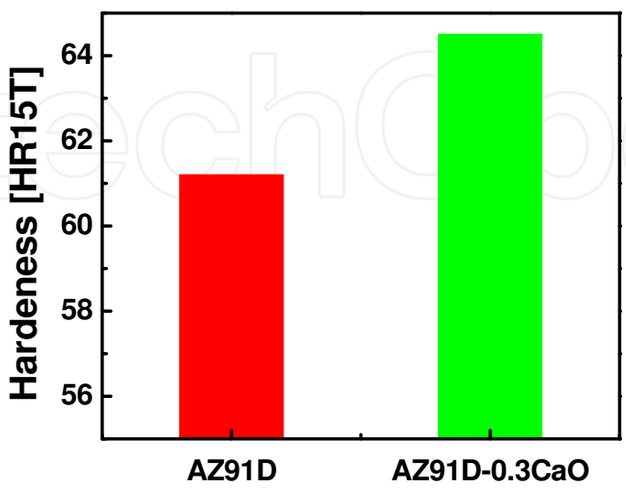

Fig. 13. Rockwell hardness values of the mechanical test specimens produced by hot chamber diecasting of AZ91D and AZ91D-0.3wt%CaO (Kim, 2009).

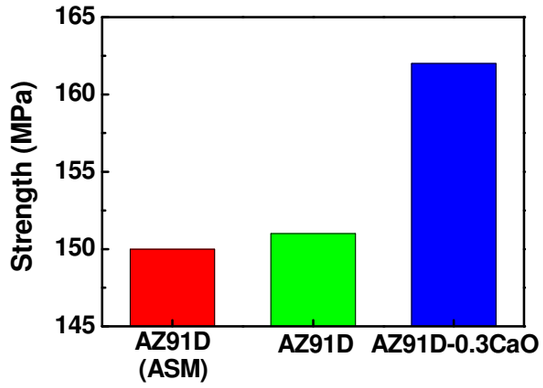

(a)

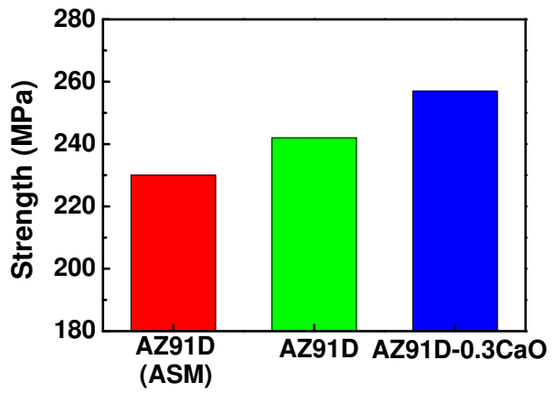

(b)

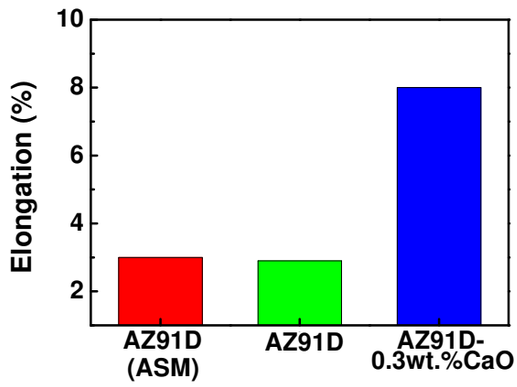

(c)

Fig. 14. Mechanical properties of the mechanical test specimens produced by hot chamber diecasting of AZ91D and AZ91D-0.3wt%CaO with the ASM reference; (a) yield strength, (b) tensile strength, (c) elongation (Kim, 2009).

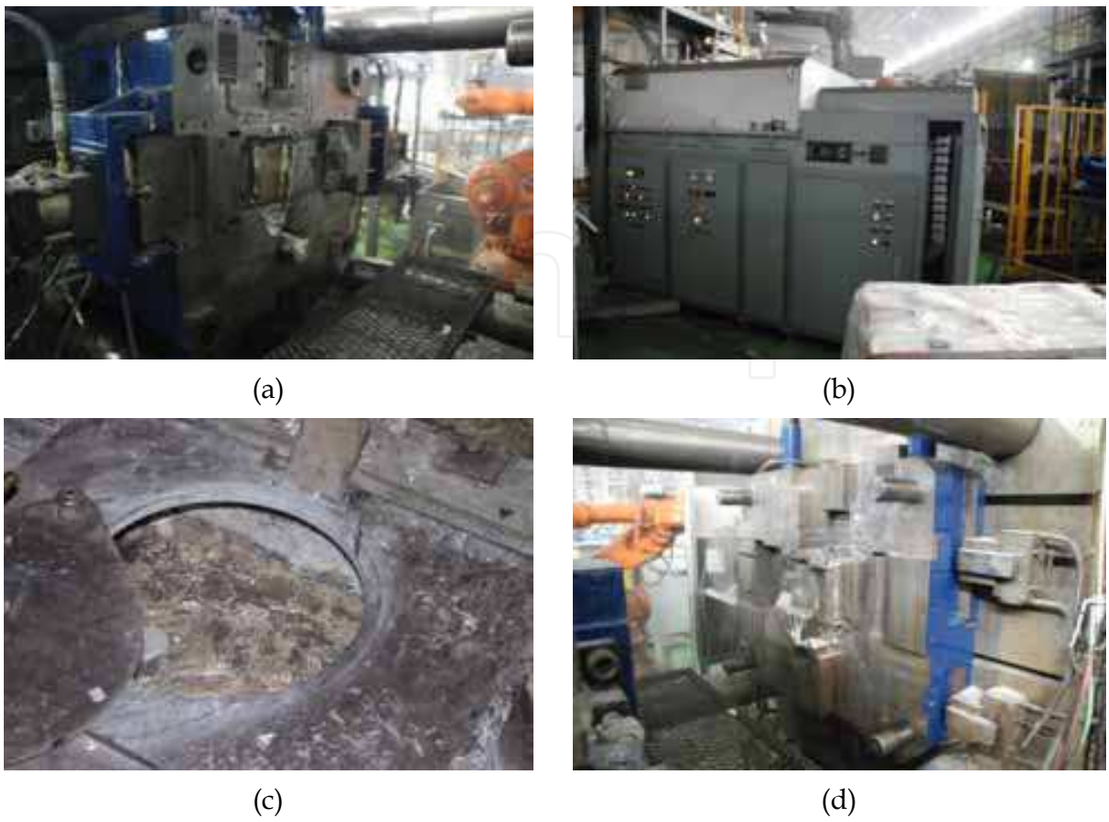

(a) (b)

(c) (d)

Fig. 15. Non-SF6 cold chamber diecasting process for CaO added AM60 Eco-Mg alloys under nitrogen atmosphere without protective gas.

(a) (b)

Fig. 16. Photograph of oil pan produced by cold chamber diecasting of (a) AM60 Eco-Mg and (b) mechanical test specimens.

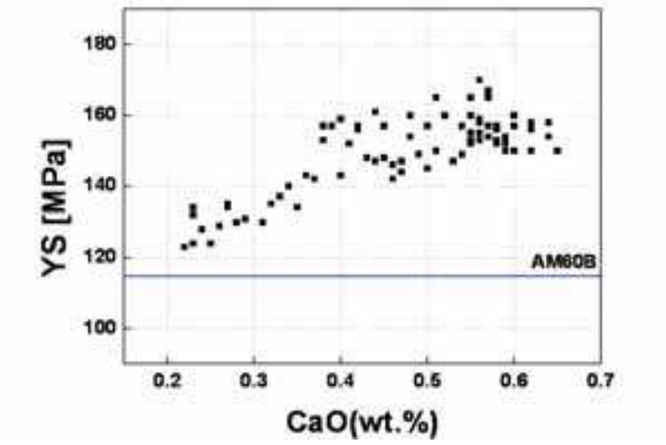

(a)

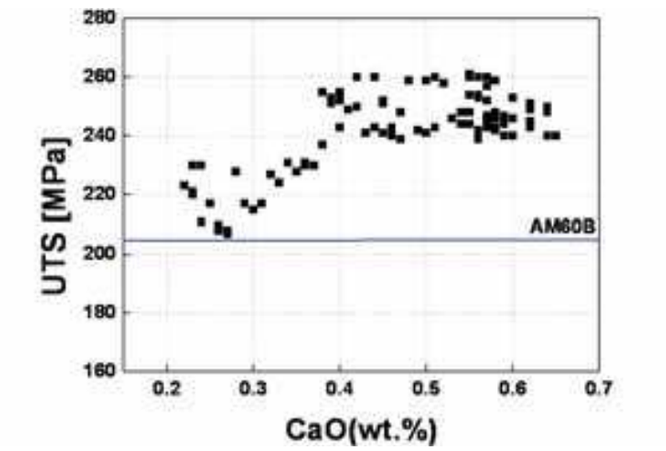

(b)

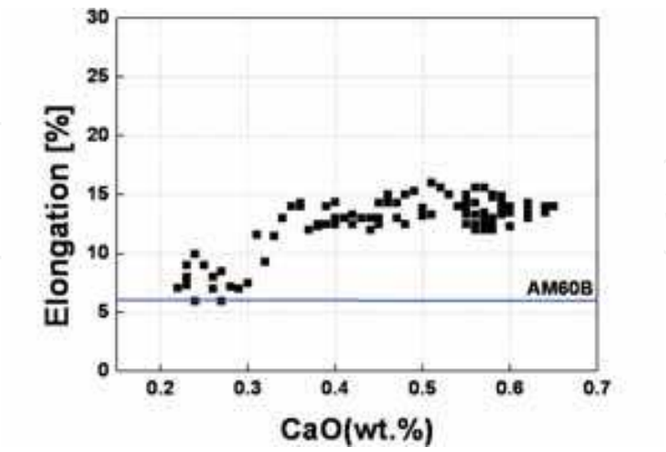

(c)

Fig. 17. Mechanical properties of mechanical test specimen produced by cold chamber diecasting of AM60 and AM60 Eco-Mg alloys at room temperature; (a) yield strength, (b) tensile strength, (c) elongation.

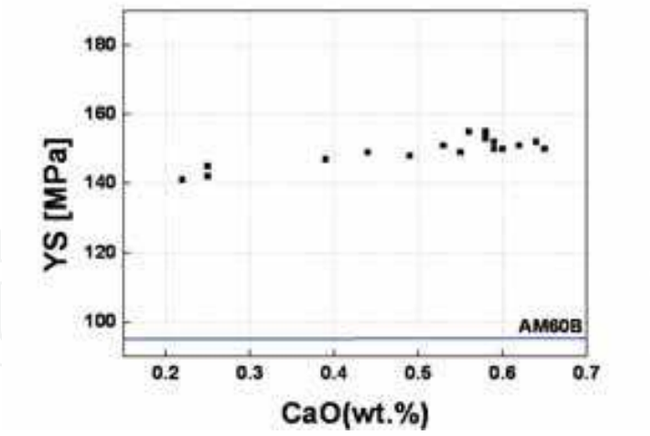

(a)

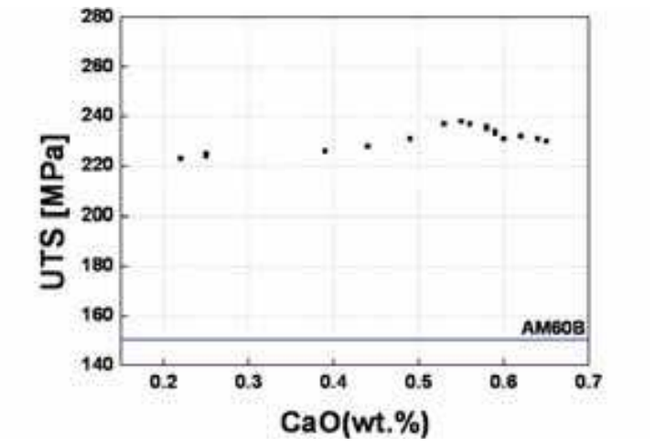

(b)

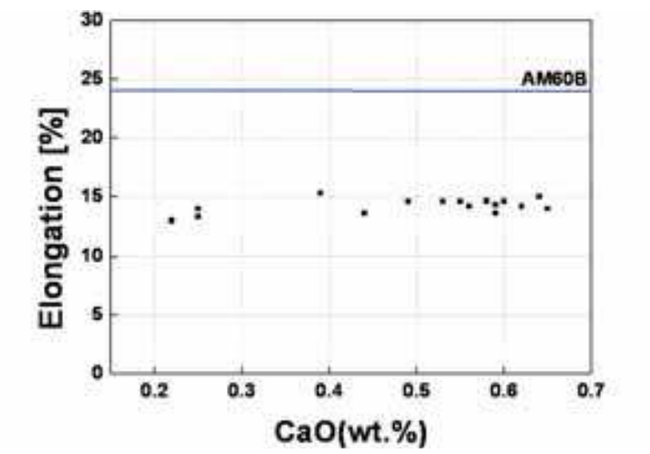

(c)

Fig. 18. Mechanical properties of mechanical test specimen produced by cold chamber diecasting of AM60 and AM60 Eco-Mg alloys at 150°C; (a) yield strength, (b) tensile strength, (c) elongation.

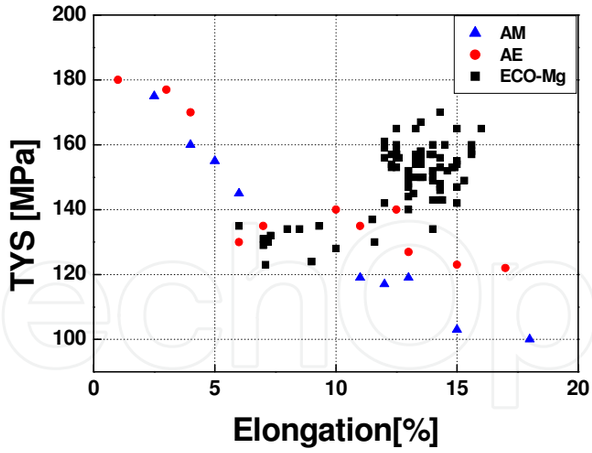

Fig. 19. Proportional strength and elongation relationship of AM60 Eco-Mg alloys.

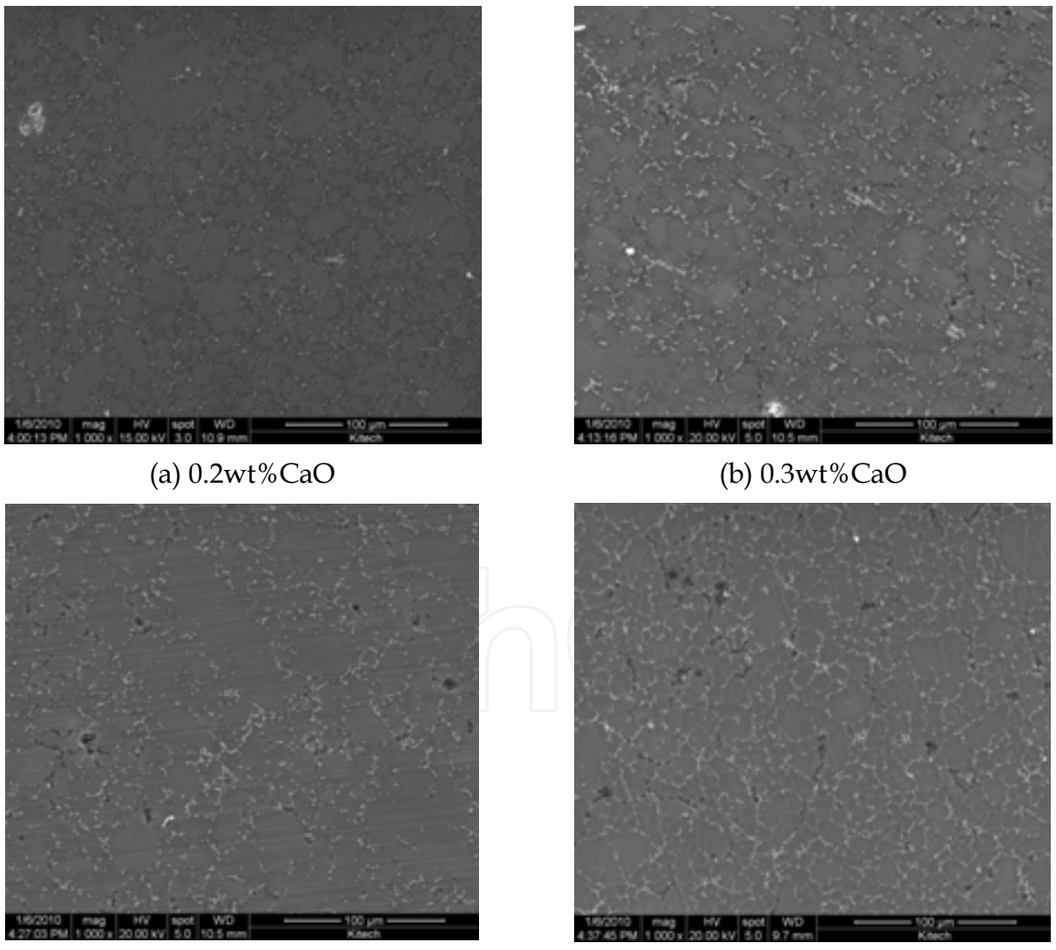

(a) 0.2wt%CaO (b) 0.3wt%CaO

(c) 0.5wt%CaO (d) 0.6wt%CaO

Fig. 20. Microstructures of (a) AM60-0.2wt%CaO, (b) AM60-0.3wt%CaO, (c) AM60-0.5wt%CaO and (d) AM60-0.6wt%CaO produced by cold chamber diecasting.

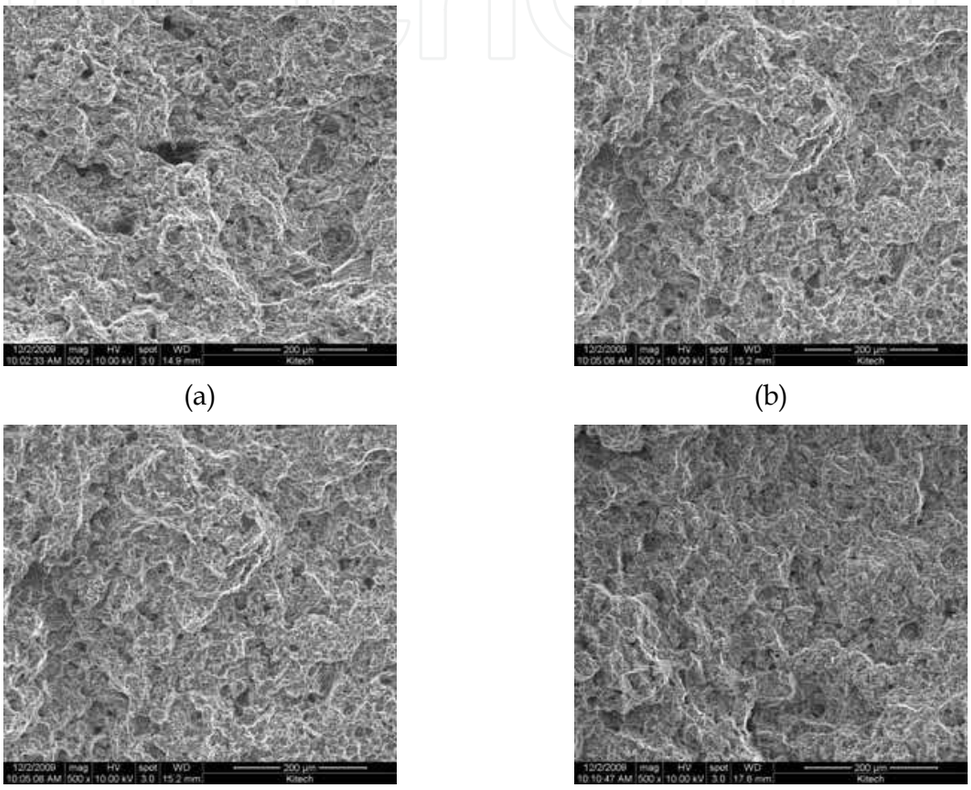

Fig. 21. SEM images of the fracture surface of tensile test specimens; (a) AM60-0.2wt%CaO, (b) AM60-0.3wt%CaO, (c) AM60-0.5wt%CaO and (d) AM60-0.6wt%CaO produced by cold chamber diecasting.

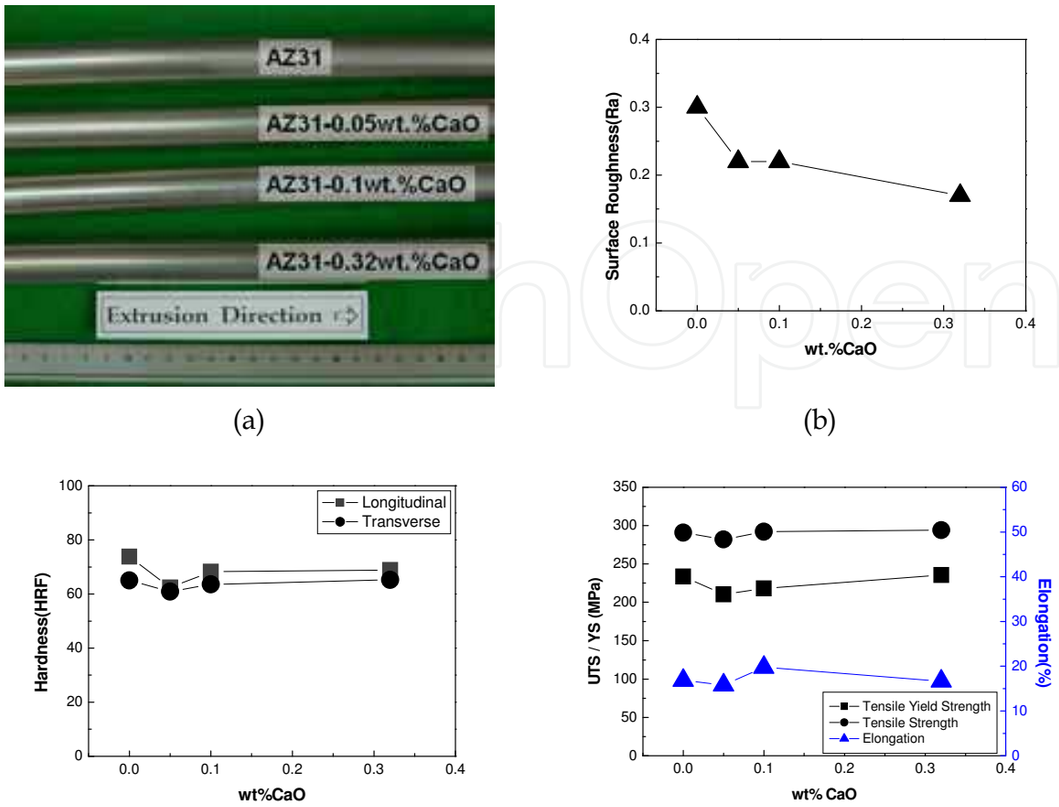

Fig. 22. (a) photographs showing the extruded bars of AZ31 and CaO added AZ31 Mg alloys and (b) surface roughness values, (c) hardness values, and (d) mechanical properties of the extruded bars (Lee, et al., 2006; Kim, 2007).

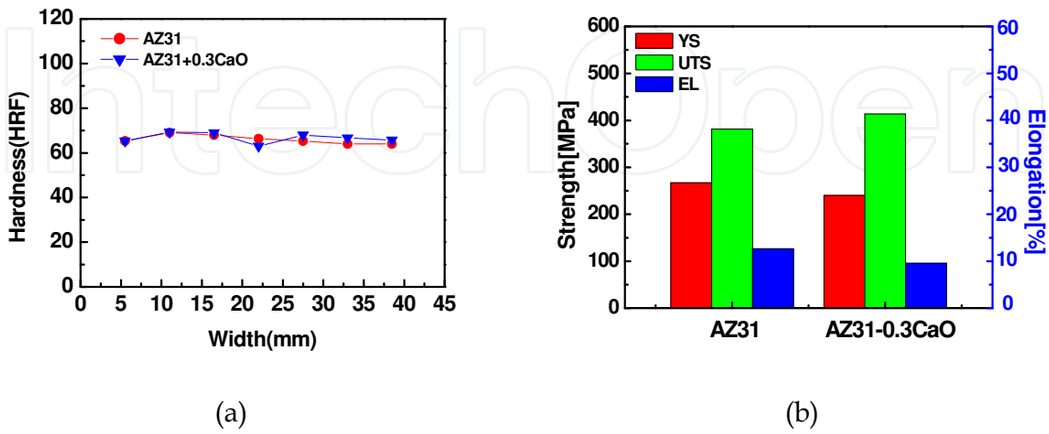

Fig. 23. (a) hardness values and (b) mechanical properties of hot-rolled AZ31 and AZ31-0.3wt%CaO Mg alloy sheets in the as-received condition (Jang, et al., 2007).

(a)

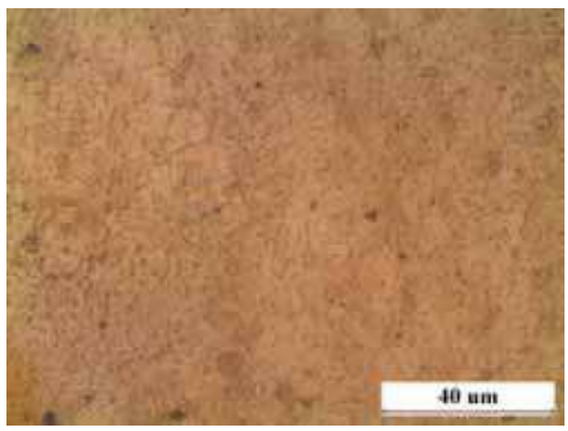

(b)

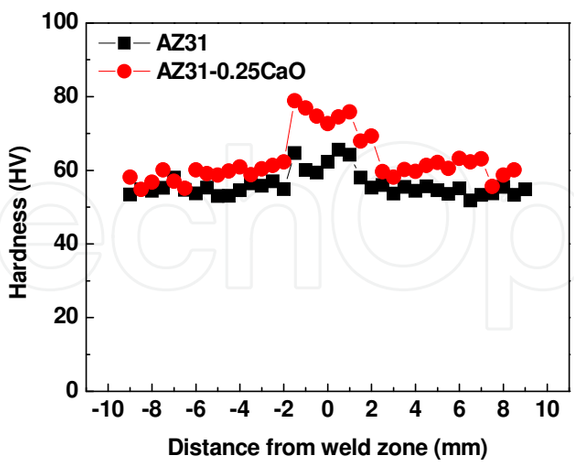

(c)

Fig. 24. Microstructures of the stir zone in (a) AZ31 and (b) AZ31-0.25wt%CaO Mg alloys and (c) hardness distribution of friction stir welded AZ31 and AZ31-0.25wt%CaO Mg alloys (Ha, et al., 2007).

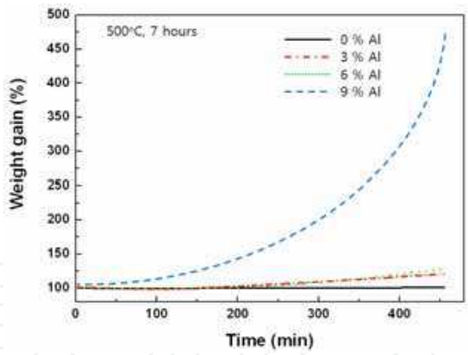

Fig. 25. Dependence of weight gain on Al content of Mg-Al Mg alloys under dry air atmosphere at 500°C for 7 hours.

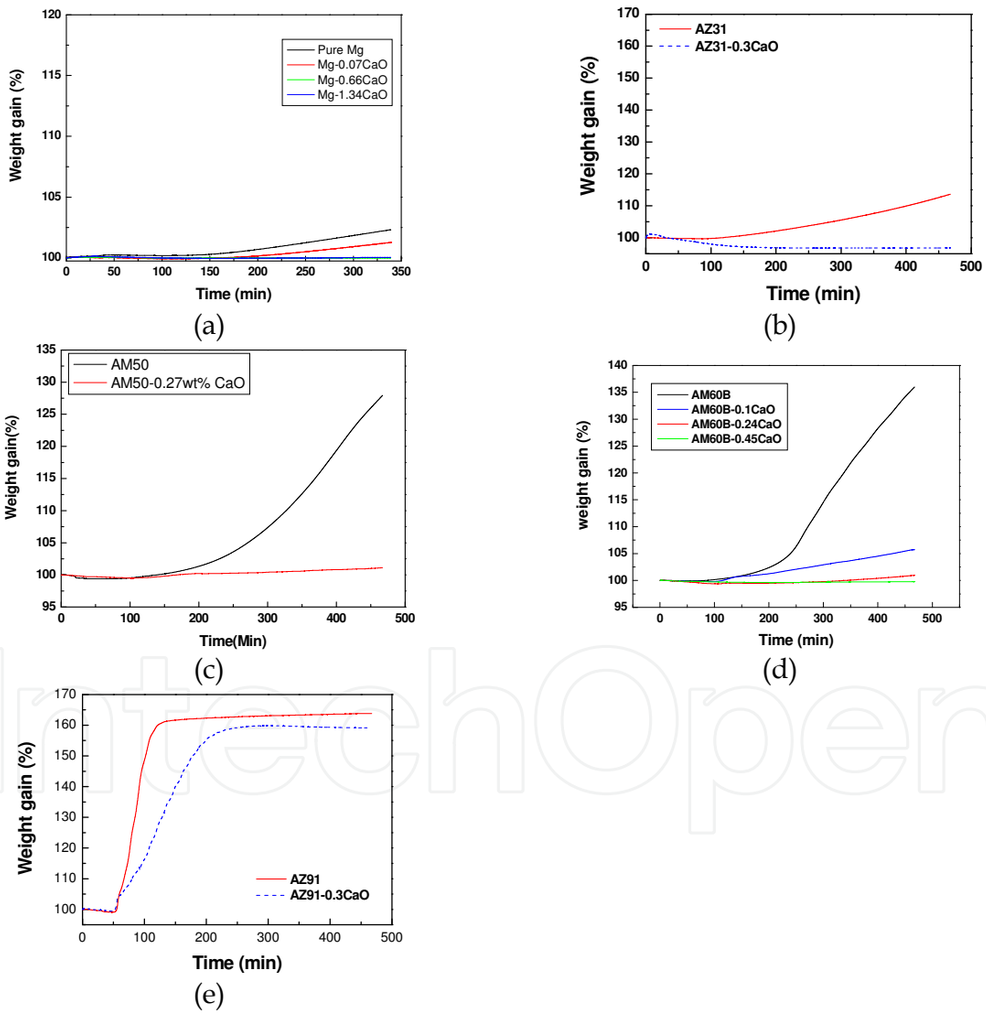

Fig. 26. Weight gain curves of (a) pure Mg, Mg-0.07wt%CaO, Mg-0.66wt%CaO, and 1.34wt%CaO, (b) AZ31 and AZ31-0.13wt%CaO, (c) AM50 and AM50-0.27wt%CaO, (d) AM60, AM60-0.1CaO, AM60-0.24wt%CaO, and AM60-0.45wt%CaO, (e) AZ91 and AZ91-0.29wt%CaO alloys (Kim, et al., 2005; Ha, et al., 2008; Lee & Kim, 2009).

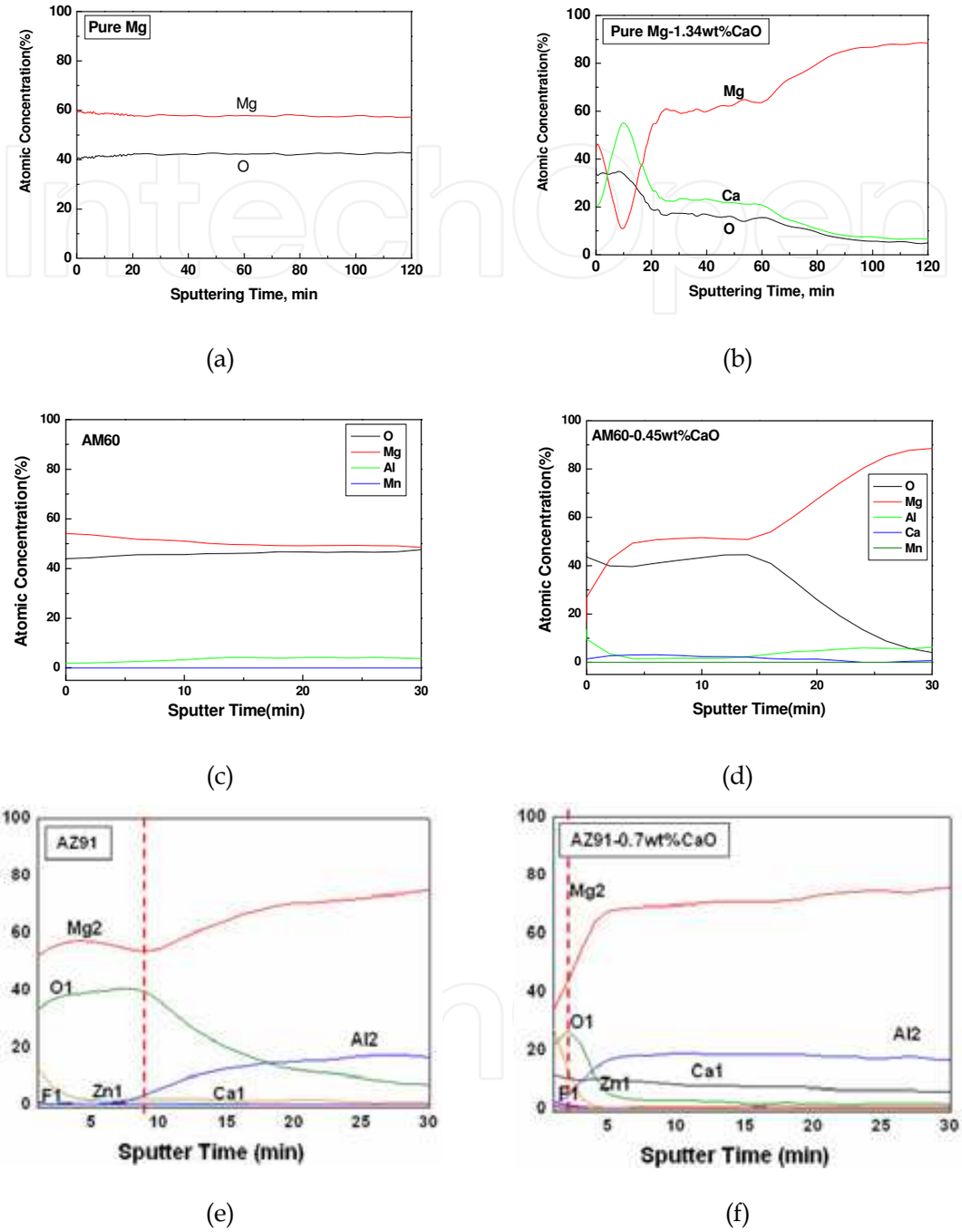

Fig. 27. AES depth profiles sputtered from the surface of (a) pure Mg, (b) Mg-1.34wt%CaO, (c) AM60, (d) AM60-0.45wt%CaO, (e) AZ91, and (f) AZ91-0.7wt%CaO alloys oxidized during TGA at 500°C for 7hours (Ha, et al., 2008; Kim, et al., 2009).

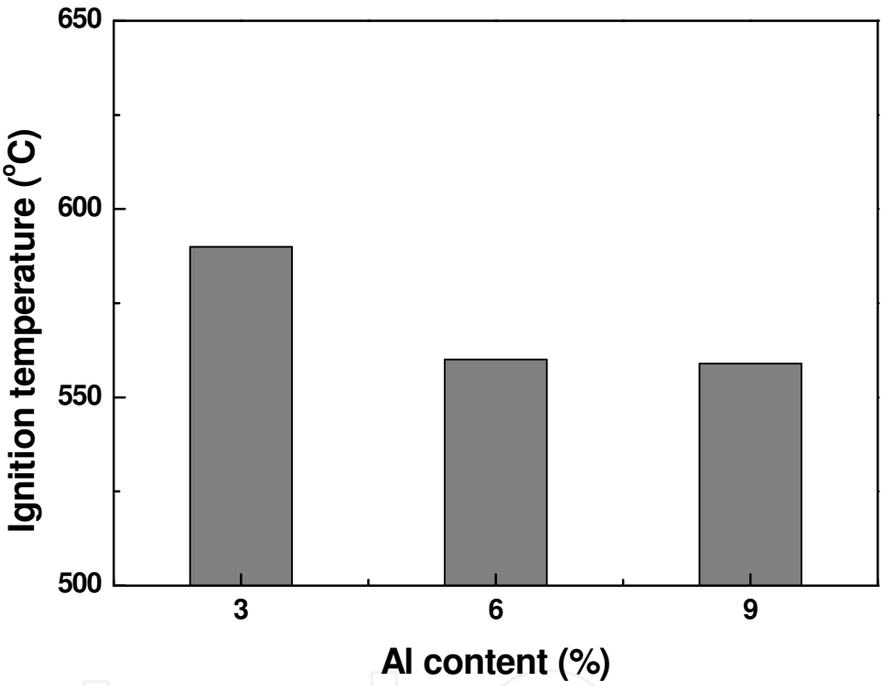

Fig. 28. Dependence of ignition temperature on Al content of Mg-Al alloys under dry air atmosphere by DTA.

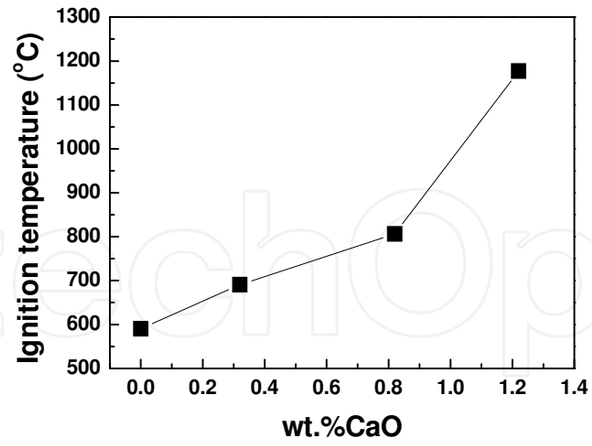

(a)

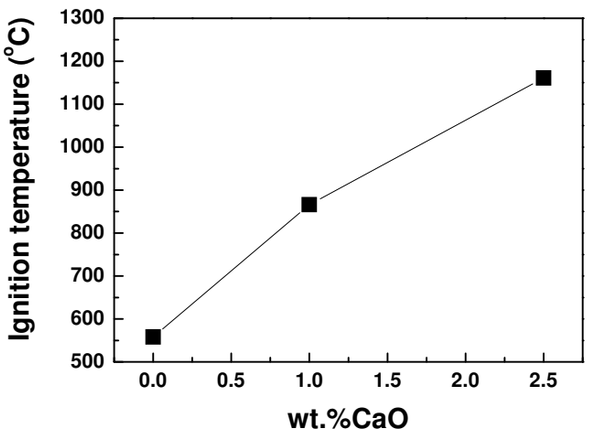

(b)

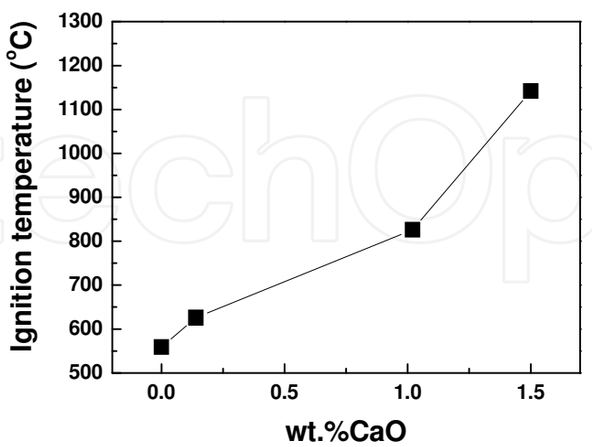

(c)

Fig. 29. Dependence of ignition temperature on CaO amount of CaO added (a) AZ31, (b) AM60, and (c) AZ91 Mg alloys under dry air atmosphere by DTA (Lee & Kim, 2009).

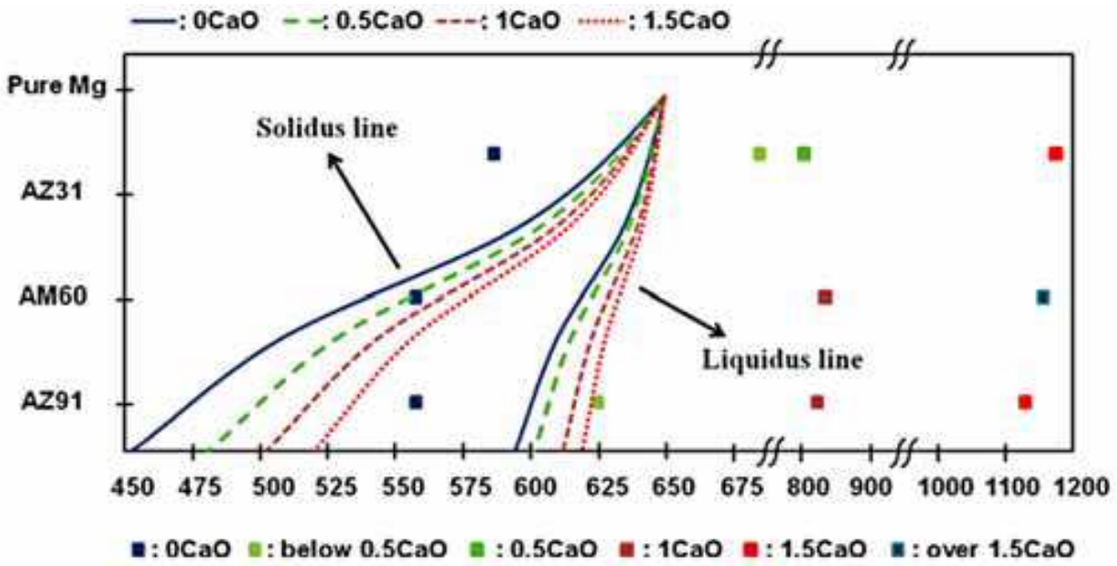

Fig. 30. Ignition temperatures for CaO added AZ31, CaO added AM60 and CaO added AZ91 Mg alloys on the solidus and liquidus lines by DTA.

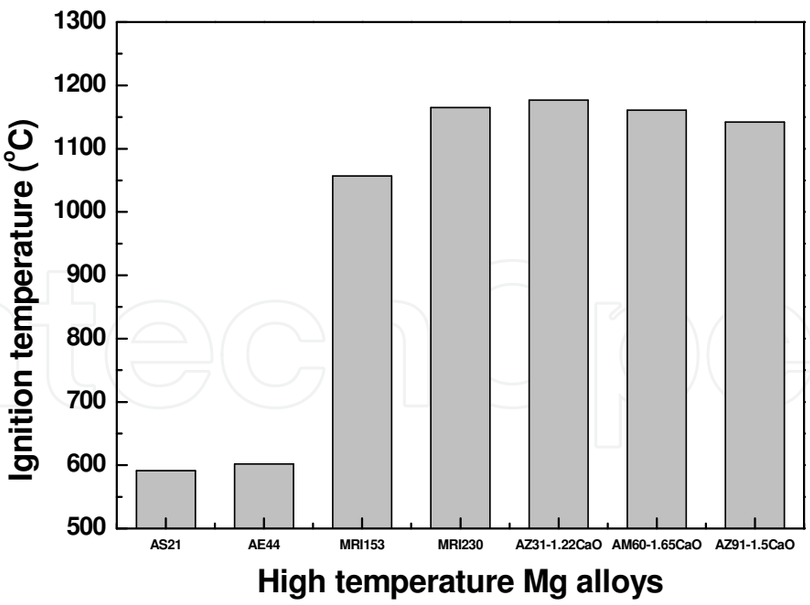

Fig. 31. Dependence of ignition temperature for AS21, AE44, MRI153, MRI230, 1.22wt%CaO added AZ31, 1.65wt%CaO added AM60, and 1.5wt%CaO added AZ91 Mg alloys under dry air atmosphere by DTA (Lee & Kim, 2009).

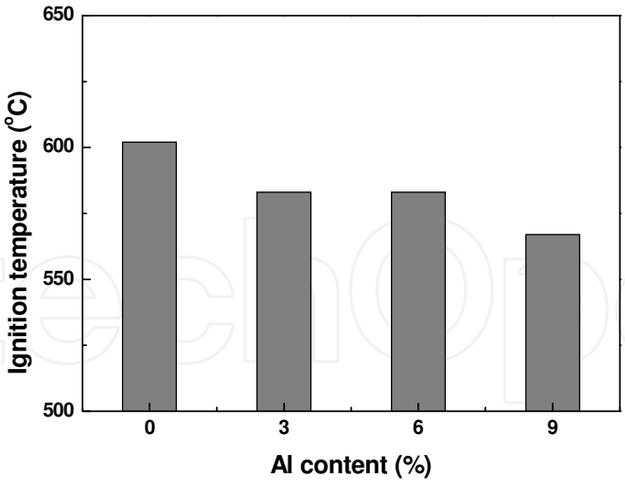

Fig. 32. Dependence of chip ignition temperatures on Al content of Mg-Al Mg alloys under an ambient atmosphere.

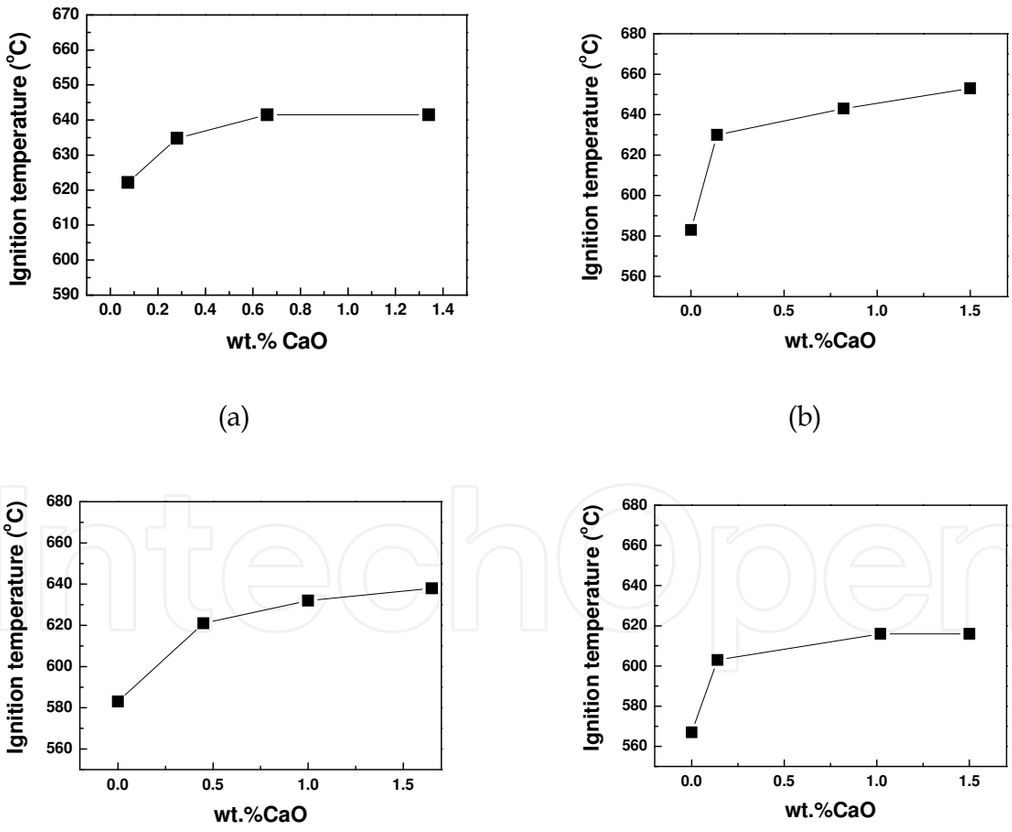

Fig. 33. Dependence of chip ignition temperatures for CaO added (a) Pure Mg, (b) AZ31, (c) AM60, and (d) AZ91 Mg alloys under an ambient atmosphere (Lee & Kim, 2009).

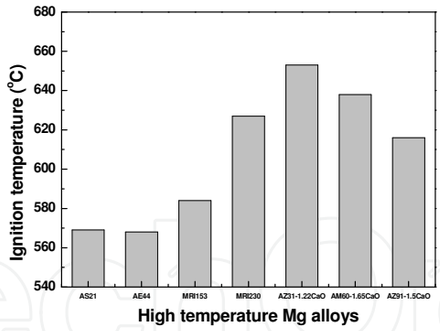

Fig. 34. Dependence of chip ignition temperatures for AS21, AE44, MRI153, MRI230, 1.22wt%CaO added AZ31, 1.65wt%CaO added AM60, 1.5wt%CaO added AZ91 Mg alloys under an ambient atmosphere (Lee & Kim, 2009).

(a) 0 sec.

(b) 30 sec.

(c) 60 sec.

(d) 90 sec.

(e) 120 sec.

(f) 150 sec.

(g) 180 sec.

(h) 210 sec.

Fig. 35. Results of torch ignition test of AZ91D and 0.3wt%CaO added AZ91 Mg alloys produced by hot-chamber diecasting (Lee & Kim, 2009).

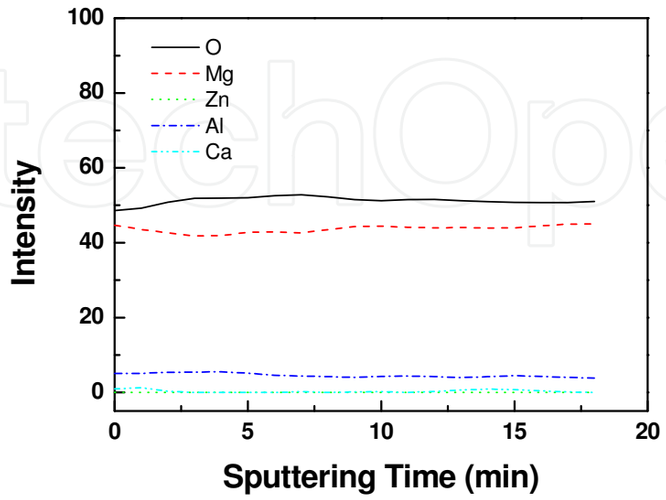

(a)

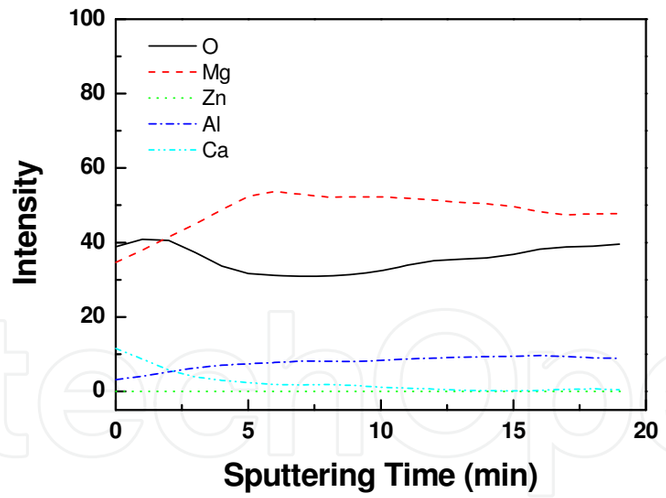

(b)

Fig. 36. AES depth profiles sputtered from the surface of (a) AZ91 and (b) 0.3wt%CaO added AZ91 Mg alloys (Lee & Kim, 2009).

Fig. 37. Results of torch ignition test of AZ31-1.13wt%CaO, AM60-1wt%CaO, AZ91-1.02wt%CaO, AS21, AE44, MRI153, and MRI230 (Lee & Kim, 2009; Lee & Kim, 2010).

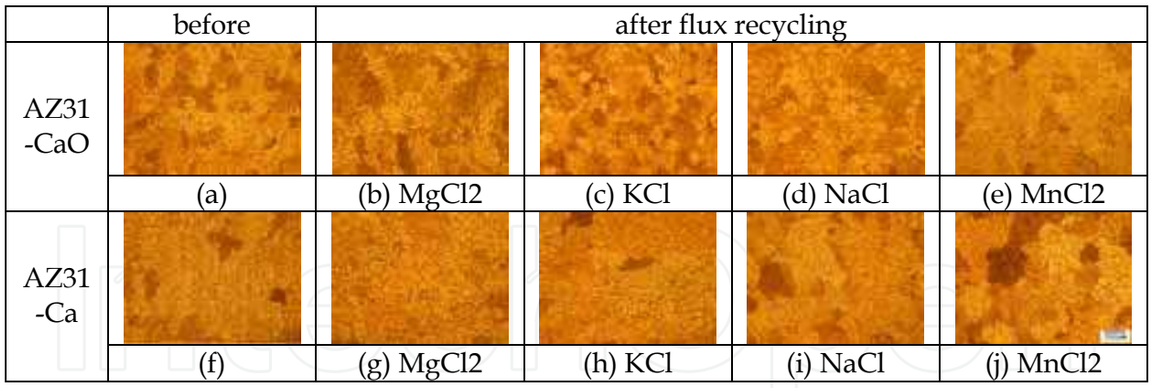

Fig. 38. As-cast microstructures of (a) AZ31-0.3wt%CaO and (f) AZ31-0.3wt%Ca and as-recycled microstructures of (b) AZ31-0.15wt%CaO after MgCl2 recycling, (c) AZ31-0.29wt%CaO after KCl recycling, (d) AZ31-0.21wt%CaO after NaCl recycling, (e) AZ31-0.10wt%CaO after MnCl2 recycling, (g) AZ31-0.12wt%Ca after MgCl2 recycling, (h) AZ31-0.25wt%Ca after KCl recycling, (i) AZ31-0.21wt%Ca after NaCl recycling, and (j) AZ31-0.10wt%Ca after MnCl2 recycling (Lee & Kim, 2009).

Alloy type	As-cast (ICP, wt%)	Flux	After recycling (ICP, wt%)	Ca loss (wt% / %)
AZ31 -0.3wt%CaO	0.29	$MgCl_2$	0.15	0.14 / 48.3
	0.30	KCl	0.29	0.01 / 3.3
	0.27	NaCl	0.21	0.06 / 22.2
	0.29	$MnCl_2$	0.10	0.19 / 65.5
AZ31 -0.3wt%Ca	0.3	$MgCl_2$	0.12	0.18 / 60.0
	0.28	KCl	0.25	0.03 / 10.7
	0.31	NaCl	0.21	0.10 / 32.3
	0.31	$MnCl_2$	0.10	0.21 / 67.7

Table 1. ICP results of CaO and Ca added AZ31 Mg alloys before and after flux recycling (Lee & Kim, 2009).

7. References

Ha, S. H.; Lee, J. K.; Yoon, Y. O.; Lee, C. Y.; Jung, S. B. & Kim, Shae K. (2007). Effect of CaO on joint properties of AZ31 alloy sheet during friction stir welding. *Proceedings of 6th International Conference on Materials Processing for Properties and Performance (MP3-2007)*, Beijing, September 2007, MP3, China

Ha, S. H.; Lee, J. K. & Kim, Shae K. (2008). Effect of CaO on oxidation resistance and microstructure of pure Mg. *Materials Transactions*, Vol. 49, No. 5 (March 2008) pp.1081-1083, ISSN 1345-9678

Jang, D. I.; Yoon, Y. O.; Kim, D. U.; Jung, S. B. & Kim, Shae K. (2007). Behavior of CaO in hot-rolled AZ31 Mg alloys. *Proceedings of 6th International Conference on Materials Processing for Properties and Performance (MP3-2007)*, Beijing, September 2007, MP3, China

Jang, D. I.; Yoon, Y. O.; Jung, S. B. & Kim, Shae K. (2008). Effect of CaO on AZ31 Mg strip castings. *Materials Transactions*, Vol. 49, No. 5 (April 2008) pp.976-979, ISSN 1345-9678

Kim, Shae K.; Lee, J. K.; Cho, H.; Jo, H. H.; Ha, W. & Kim, Y. J. (2005). The behavior of CaO in magnesium alloys. *Magnesium Technology 2005* (TMS-2005), Neale R. N., pp. 285-289, ISBN 0-87339-582-4, San Francisco, February 2005, USA

Kim, Shae K.; Lee, J. K.; Yoon, Y. O.; & Jo, H. H. (2007). Development of AZ31 Mg alloy wrought process route without protective gas. *Journal of Materials Processing Technology*, Vol. 187-188, pp. 757-760, ISSN 0924-0136

Kim, Shae K.; Lee, J. K.; Jang D. I.; Yoon, Y. O.; Ha, S. H.; Yoo, H. J.; Park, S. M.; Lee, C. H. & Kim, Y. J (2009). Eco-Mg for magnesium future. *Proceedings of 66th Annual World Magnesium Conference (IMA-2009)*, San Francisco, May 2009, IMA, USA

Kim, Shae K. (2009). Non-SF6 diecasting process of 0.3wt%CaO added AZ91D Mg alloy. *Proceedings of 18th International Conference on Processing and Fabrication and Advanced Materials (PFAM18-2009)*, Sendai, December 2009, PFAM18, Japan

Kim, Shae K. (2009). Effect of Al content on phase formation of CaO added Mg alloy. *Proceedings of 18th International Conference on Processing and Fabrication and Advanced Materials (PFAM18-2009)*, Sendai, December 2009, PFAM18, Japan

Lee, J. K.; Yoon, Y. O. & Kim, Shae K. (2006). Development of CaO added wrought Mg alloy for cleaner production. *Magnesium Technology 2006* (TMS-2006), Neale R. N., pp. 517-521, ISBN 978-0-87339-620-2, San Antonio, March 2006, USA

Lee, J. K.; Ha, S. H.; Kim, Y. J.; Jo, H. H. & Kim, Shae K. (2007). Melt protection property and ignition resistance property of CaO added AZ91D Mg alloy. *Journal of the Korean Foundrymen's Society*, Vol. 27, No. 3, pp. 131-134, ISSN 1598-706X

Lee, J. K. & Kim, Shae K. (2008). Development of novel environment-friendly magnesium alloys. *Advanced Materials Research*, Vol.47-50, pp. 940-943, ISSN 1022-6680

Lee, J. K. & Kim, Shae K. (2009). Thermodynamic consideration of CaO added Mg alloys in recycling process. *Materials Science Forum*, Vol. 620-622, (January 2009) pp. 615-618

Lee, J. K. & Kim, Shae K. (2009). Flame resistance behaviors of AS, AE, MRI and AO series Mg alloys. *Magnesium Technology 2009* (TMS-2009), Eric A. N., pp. 155-159, ISBN 978-0-87339-730-8, San Francisco, February 2009, USA

Lee, J. K. & Kim, Shae K. (2009). Flame resistance of 0.3wt%CaO added AZ91D Mg alloy manufactured by diecasting process. *Proceedings of 18th International Conference on Processing and Fabrication and Advanced Materials (PFAM18-2009)*, Sendai, December 2009, PFAM18, Japan

Lee, J. K. & Kim, Shae K. (2009). Oxidation resistance behaviour of CaO added Mg-Al alloys. *Proceedings of 18th International Conference on Processing and Fabrication and Advanced Materials (PFAM18-2009)*, Sendai, December 2009, PFAM18, Japan

Lee, J. K. & Kim, Shae K. (2010). Fire-proof evaluation of CaO added Mg-3Al, Mg-6Al, and Mg-9Al Mg cast products. *Magnesium Technology 2010* (TMS-2010), Sean R. A, pp. 121-128, ISBN 978-0-87339-746-9, Seattle, February 2010, USA

Pilling, N. B. & Bedworth, R. E. (1923). The oxidation of metals in high temperature. Journal of Institute of Metals, Vol. 29, pp. 529-582

You, B. S.; Park, W. W. & Chung, I. S. (2000). The effect of calcium additions on the oxidation behaviour in magnesium alloys. Scripta Materialia, Vol. 42, pp. 1089-1094, ISSN 1359-6462

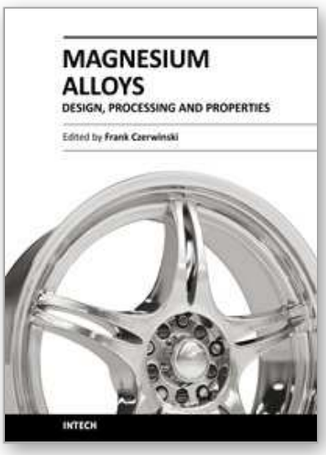

Magnesium Alloys - Design, Processing and Properties

Edited by Frank Czerwinski

ISBN 978-953-307-520-4
Hard cover, 526 pages
Publisher InTech
Published online 14, January, 2011
Published in print edition January, 2011

Scientists and engineers for decades searched to utilize magnesium, known of its low density, for light-weighting in many industrial sectors. This book provides a broad review of recent global developments in theory and practice of modern magnesium alloys. It covers fundamental aspects of alloy strengthening, recrystallization, details of microstructure and a unique role of grain refinement. The theory is linked with elements of alloy design and specific properties, including fatigue and creep resistance. Also technologies of alloy formation and processing, such as sheet rolling, semi-solid forming, welding and joining are considered. An opportunity of creation the metal matrix composite based on magnesium matrix is described along with carbon nanotubes as an effective reinforcement. A mixture of science and technology makes this book very useful for professionals from academia and industry.

INTECH
open science | open minds

InTech Europe
University Campus STeP Ri
Slavka Krautzeka 83/A
51000 Rijeka, Croatia
Phone: +385 (51) 770 447
Fax: +385 (51) 686 166
www.intechopen.com

InTech China
Unit 405, Office Block, Hotel Equatorial Shanghai
No.65, Yan An Road (West), Shanghai, 200040, China
中国上海市延安西路65号上海国际贵都大饭店办公楼405单元
Phone: +86-21-62489820
Fax: +86-21-62489821

IntechOpen